Article

Cell Reports

Restricting Glycolysis Preserves T Cell Effector Functions and Augments Checkpoint Therapy

Graphical Abstract

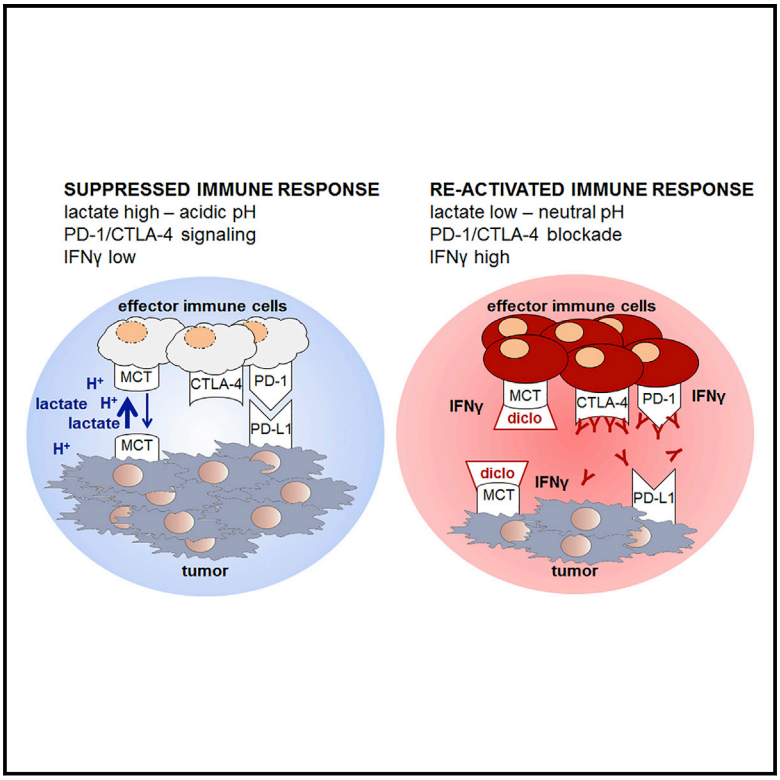

Authors

Kathrin Renner, Christina Bruss, Annette Schnell, ..., Katja Dettmer, Mark Selby, Marina Kreutz

Correspondence

kathrin.renner-sattler@ukr.de

In Brief

Renner et al. demonstrate a negative correlation between glycolytic activity in tumors and response to checkpoint therapy. Genetic blockade of glycolysis or pharmacological inhibition of the main lactate transporters MCT1 and MCT4 preserves T cell function, reverses tumor acidification, and augments response to checkpoint therapy.

Highlights

- Glycolytic index in melanoma negatively correlates with response to anti-PD1 therapy
- Blocking lactate transport or knock out of glycolytic genes improves checkpoint therapy
- Diclofenac blocks the lactate transporters MCT1 and MCT4 in a COX-independent manner
- Inhibition of glycolysis by MCT blockade does not impede T cell function

Renner et al., 2019, Cell Reports *29*, 135–150
October 1, 2019
https://doi.org/10.1016/j.celrep.2019.08.068

CellPress

Cell Reports
Article

Restricting Glycolysis Preserves T Cell Effector Functions and Augments Checkpoint Therapy

Kathrin Renner,[1,2,21,24,*] Christina Bruss,[1,21] Annette Schnell,[1,21] Gudrun Koehl,[3] Holger M. Becker,[4,22] Matthias Fante,[1] Ayse-Nur Menevse,[2] Nathalie Kauer,[1] Raquel Blazquez,[1] Lisa Hacker,[1] Sonja-Maria Decking,[1] Toszka Bohn,[5] Stephanie Faerber,[1] Katja Evert,[6] Lisa Aigle,[1] Sabine Amslinger,[7] Maria Landa,[7,23] Oscar Krijgsman,[8] Elisa A. Rozeman,[8] Christina Brummer,[1] Peter J. Siska,[1] Katrin Singer,[1] Stefanie Pektor,[9] Matthias Miederer,[9] Katrin Peter,[1] Eva Gottfried,[1] Wolfgang Herr,[1] Ibtisam Marchiq,[10] Jacques Pouyssegur,[10,11] William R. Roush,[12] SuFey Ong,[13] Sarah Warren,[13] Tobias Pukrop,[1] Philipp Beckhove,[2] Sven A. Lang,[14] Tobias Bopp,[5,15,16,17] Christian U. Blank,[8] John L. Cleveland,[18] Peter J. Oefner,[19] Katja Dettmer,[19] Mark Selby,[20] and Marina Kreutz[1,2]

[1]Department of Internal Medicine III, University Hospital Regensburg, Regensburg, Germany
[2]Regensburg Center for Interventional Immunology, Regensburg, Germany
[3]Department of Surgery, University Hospital Regensburg, Regensburg, Germany
[4]Division of General Zoology, University of Kaiserslautern, Kaiserslautern, Germany
[5]Institute for Immunology, University Medical Center Johannes Gutenberg University (UMC) Mainz, Mainz, Germany
[6]Institute of Pathology, University of Regensburg, Regensburg, Germany
[7]Institute of Organic Chemistry, University of Regensburg, Regensburg, Germany
[8]Department Medical Oncology and Division of Molecular Oncology and Immunology, The Netherlands Cancer Institute, Amsterdam, the Netherlands
[9]Department of Nuclear Medicine, University Medical Center, Johannes Gutenberg University Mainz, Mainz, Germany
[10]Institute of Research on Cancer and Aging (IRCAN), CNRS-INSERM-UNS UMR 7284, Nice, France
[11]Department of Medical Biology, Scientific Centre of Monaco (CSM), Monaco
[12]Department of Chemistry, The Scripps Research Institute, Scripps-Florida, Jupiter, FL, USA
[13]NanoString Technologies, Seattle, WA, USA
[14]Department of General and Visceral Surgery, Medical Center, Faculty of Medicine University of Freiburg, Freiburg, Germany
[15]Research Center for Immunotherapy (FZI), UMC Mainz, Mainz, Germany
[16]University Cancer Center Mainz, UMC Mainz, Mainz, Germany
[17]German Cancer Consortium (DKTK), Heidelberg, Germany
[18]Department of Tumor Biology, Moffitt Cancer Center and Research Institute, Tampa, FL, USA
[19]Institute of Functional Genomics, University of Regensburg, Regensburg, Germany
[20]Bristol-Myers Squibb, Redwood City, CA, USA
[21]These authors contributed equally
[22]Present address: Department of Physiological Chemistry, University of Veterinary Medicine Hannover, Hannover, Germany
[23]Present address: Institute of Organic Chemistry, University of Stuttgart, Stuttgart, Germany
[24]Lead Contact
*Correspondence: kathrin.renner-sattler@ukr.de
https://doi.org/10.1016/j.celrep.2019.08.068

SUMMARY

Tumor-derived lactic acid inhibits T and natural killer (NK) cell function and, thereby, tumor immunosurveillance. Here, we report that melanoma patients with high expression of glycolysis-related genes show a worse progression free survival upon anti-PD1 treatment. The non-steroidal anti-inflammatory drug (NSAID) diclofenac lowers lactate secretion of tumor cells and improves anti-PD1-induced T cell killing *in vitro*. Surprisingly, diclofenac, but not other NSAIDs, turns out to be a potent inhibitor of the lactate transporters monocarboxylate transporter 1 and 4 and diminishes lactate efflux. Notably, T cell activation, viability, and effector functions are preserved under diclofenac treatment and in a low glucose environment *in vitro*. Diclofenac, but not aspirin, delays tumor growth and improves the efficacy of checkpoint therapy *in vivo*. Moreover, genetic suppression of glycolysis in tumor cells strongly improves checkpoint therapy. These findings support the rationale for targeting glycolysis in patients with high glycolytic tumors together with checkpoint inhibitors in clinical trials.

INTRODUCTION

Immunotherapy with immune checkpoint inhibitors can overcome T cell anergy and activate the anti-tumor immune response, and yet, many patients still fail on such therapies (Balar and Weber, 2017; Migali et al., 2016; Sharma et al., 2017; Zhao and Subramanian, 2017). The tumor microenvironment is also characterized by nutrient competition and accumulation of metabolites, which compromise T cell metabolism and function and might contribute to the restricted response to checkpoint

blockade (Anderson et al., 2017; Brand et al., 2016; Chang et al., 2015; Colegio et al., 2014; Ho et al., 2015). Accordingly, combination strategies are being developed to target both metabolism and immune checkpoints. Interestingly, the combination of immune checkpoint inhibition with the non-steroidal anti-inflammatory drug (NSAID) aspirin, which blocks cyclooxygenase (COX) activity and prostaglandin E secretion (PGE_2), has been shown to augment the efficacy of checkpoint blockade (Zelenay et al., 2015). However, in addition to elevated lipid metabolism and COX expression, tumor cells are often characterized by increased glycolytic activity that results in intratumoral lactate accumulation and acidification. Furthermore, T and natural killer (NK) cells take up lactic acid that impairs effector functions (Fischer et al., 2007). Accordingly, strategies that impair tumor cell glycolysis improve immunosurveillance and tumor growth control (Brand et al., 2016; Long et al., 2018). In line with these findings, tumor glucose fermentation inversely correlates with T cell infiltration and overall survival (Ottensmeier et al., 2016; Singer et al., 2011). Moreover, retrospective analyses have shown that elevated lactate dehydrogenase (LDH) correlates with poor prognosis and outcome in anti-PD1-treated patients (Heppt et al., 2017; Kelderman et al., 2014; Wen et al., 2017).

Given these findings, there are efforts to develop effective means to impair tumor glycolysis in order to improve the response to checkpoint therapy. Targeting lactate transporters (monocarboxylate transporters [MCTs]) is a promising approach (Baek et al., 2014; Doherty et al., 2014; Long et al., 2018; Marchiq et al., 2015). Indeed, MCT1/2-selective inhibitors rapidly disable glycolysis (Baek et al., 2014; Doherty et al., 2014; Marchiq et al., 2015) and are currently tested in a phase 1 trial (https://www.clinicaltrials.gov/ct2/show/NCT01791595). However, the efficacy of such agents in reducing tumor cell lactate efflux can be limited by co-expression of MCT4, which is frequently found on tumor cells (Doherty et al., 2014; Le Floch et al., 2011; Marchiq et al., 2015). Therefore, the simultaneous inhibition of MCT1/2 and MCT4 transporters is likely required to significantly reduce lactic acid secretion in the tumor milieu. Such agents could also target immune cell metabolism and, thereby, impair their function, as increases in glycolysis have been linked to the effector functions e.g. of T cells (Chang et al., 2013; Freemerman et al., 2014; Gubser et al., 2013; Kelly and O'Neill, 2015; Macintyre et al., 2014; van der Windt and Pearce, 2012). However, a recent study has shown that the response to adoptive T cell transfer can be improved by glycolytic inhibitors (Cascone et al., 2018) and genetic downregulation of the lactate-generating enzyme LDHA improved the efficacy of anti-PD-1 treatment (Daneshmandi et al., 2019).

Here, we tested the hypothesis whether pharmacological targeting of tumor glycolysis could improve checkpoint blockade. In support of this notion, a high glycolytic index negatively correlated with progression-free survival in cancer patients treated with anti-PD1 therapy. As diclofenac targets glucose metabolism not only in murine tumor models and cell lines but also in patients with actinic keratosis (Gottfried et al., 2013; Singer et al., 2019), we tested its impact on the efficacy of checkpoint therapy.

T-cell-mediated killing of tumor cells could be improved in an *in vitro* coculture assay by pre-treating tumor cells with diclofenac, which we identified as a potent inhibitor of MCT1 and MCT4. Diclofenac spared the anti-tumor activity of effector T cells *in vitro* and improved checkpoint therapy in two tumor models. These findings support the concept of combining diclofenac or other MCT inhibitors with immunotherapy.

RESULTS

Tumor Cell Glycolysis Limits the Response to Checkpoint Inhibition

We investigated whether local metabolic activity affects the response to checkpoint therapy in biopsies of 47 melanoma patients prior to anti-PD-1 treatment (Table S1). A glycolytic index based on the expression level of glycolysis-related genes was calculated (Table S2) (https://meetinglibrary.asco.org/record/156550/abstract). Patients with lower index levels had an increased probability of longer progression-free survival times (Figure 1A), even after adjustment for sex, age, pre-treatment, stage, and location.

These patient data suggested that increased glycolytic activity limits the efficacy of checkpoint therapy. Thus, targeting glucose fermentation could improve response rates. As lactic acid inhibits T-cell-mediated killing (Brand et al., 2016), we investigated whether reducing lactate secretion improves T-cell-mediated killing of melanoma and pancreatic tumor cells in combination with PD-L1 knockdown, resembling the application of anti-PD-1 antibodies. As we have previously shown that diclofenac impairs lactate efflux of tumor cells (Gottfried et al., 2013), melanoma (M579) and pancreatic cancer cells (PANC-1) were pretreated with diclofenac. Diclofenac diminished lactate secretion in both tumor cell lines (Figure 1B) independent of any effect on proliferation, as shown by normalization to cell number applying the consumption and release profiling (CORE) method (Figure S1A; Jain et al., 2012). The viability of tumor cells and T cells was not affected by 72 h of diclofenac treatment (Figures S1B and S1C). More lactate was detected in supernatants of melanoma cells compared to pancreatic cancer cells (Figure 1B). T cells alone were not capable of killing tumor cells in both model systems (Figure 1C). PD-L1 knockdown was effective (Figure 1D) but by itself insufficient to induce T-cell-mediated melanoma cell killing (Figure 1C). High concentrations of lactic acid might suppress responses to checkpoint blockade. In line, reduction of lactate secretion through diclofenac boosted T-cell-mediated killing in PD-L1 knocked down melanoma cells (Figure 1C). In contrast, aspirin, ketoprofen, or lumiracoxib had only a limited effect on lactate secretion and killing (Figures 1E and 1F). In contrast to melanoma cells, PD-L1 knockdown in pancreatic cancer cells boosted T-cell-mediated killing (Figure 1C), which was further enhanced by diclofenac. Adding lactic acid in tumor-relevant concentrations reverted the positive effect of diclofenac (Figure 1G). This effect can be explained by the fact that T cells died under increasing lactic acid concentrations (Figure S1D), whereas pancreatic tumor cells tolerated the exogenous addition of lactic acid in contrast to M579 cells (Figure S1C). Taken together, reducing tumor efflux of lactate enhances the immune response to checkpoint inhibition.

Diclofenac Directly Inhibits MCT1 and MCT4 Activity

As some NSAIDs, including diclofenac, are monocarboxylates, we hypothesized that diclofenac directly targets MCTs. We

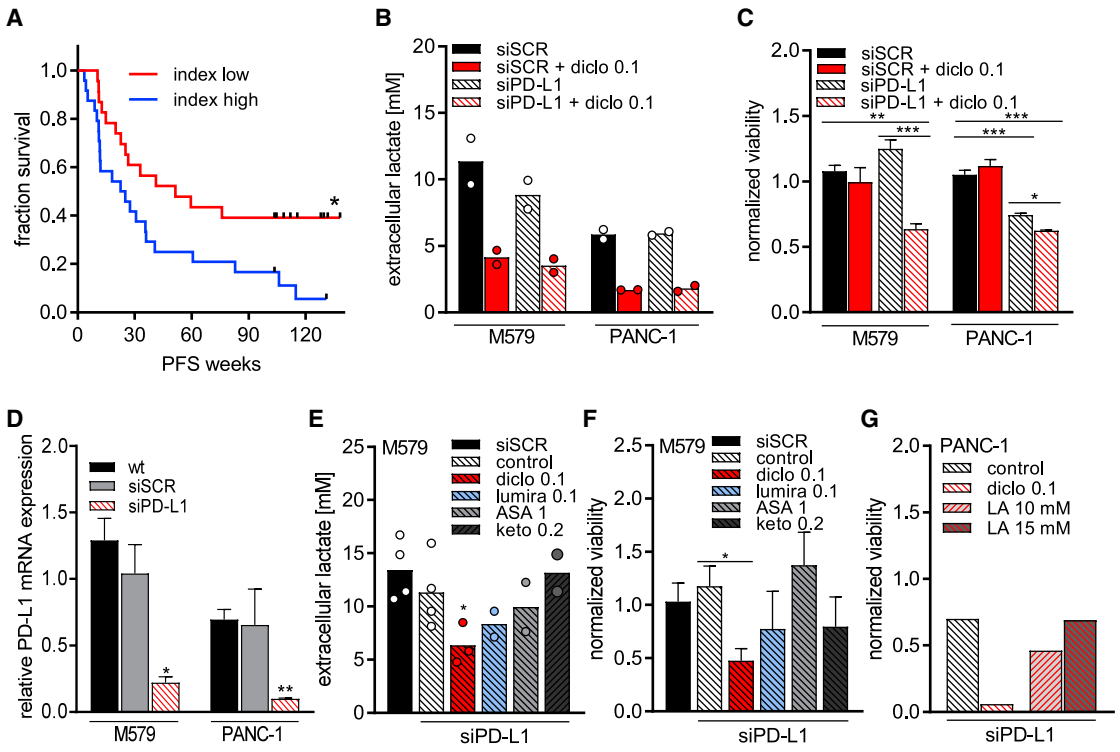

Figure 1. Glycolytic Activity Limits T Cell Response

(A) Expression of AKT1, HIF1A, SLC2A1, HK2, HK1, TPI1, ENO1, LDHA, PFKFB3, PFKM, GOT1, GOT2, and GLUD1 was analyzed in melanoma biopsies of 47 patients prior to anti-PD1 therapy, and a glycolytic index was calculated. Patients were stratified according to the median index calculated; progression-free survival was plotted as a Kaplan Meier estimation curve. Significance was calculated applying the log-rank (Mantel-Cox) test.

(B–G) M579-LUC or PANC-1-LUC cells were transfected either with pools of small interfering RNA (siRNA) either scrambled (siSCR) or siRNAs targeting PD-L1 (siPD-L1).

(B) Lactate levels in supernatants were determined after 72 h of transfection in the presence or absence of 0.1 mM diclofenac. The experiment was conducted twice; each time two independent plates with four technical replicates were performed. Supernatants of technical replicates were pooled for analysis (mean, n = 2).

(C) 72 h after transfection, tumor cells were pulsed with influenza peptide and influenza-specific T (FluT) cells were added, and after 20 h of coculture, luciferase activity of tumor cells was determined. Tumor cell viability was calculated as the ratio of luciferase activity of tumor cells only to tumor cells cocultured with FluT cells within one treatment condition. The experiment was conducted two times; each time two independent plates with four technical replicates on each were performed. Mean of technical replicates of each plate was calculated (one-way ANOVA, Dunnett's multiple comparisons test, $*p < 0.05$, $**p < 0.01$, $***p < 0.001$, mean + SEM, n = 4).

(D) PD-L1 mRNA expression was analyzed in wild-type cells (WT), in cells treated with siSCR and cells treated with siPD-L1 (one-way ANOVA paired, Dunnett's multiple comparisons test, $*p < 0.05$, $**p < 0.01$, mean + SEM, n = 4).

(E and F) M579 cells were transfected as indicated in the presence or absence of 0.1 mM diclofenac (diclo), 0.1 mM lumiracoxib (lumira), 1 mM aspirin (ASA), or 0.2 mM ketoprofen (keto).

(E) Lactate levels were determined in supernatants after 72 h of transfection (mean, n = 2 to 4).

(F) 72 h after transfection, tumor cells were pulsed with influenza peptide, peptide was removed, and medium only or FluT was added. After 20 h, luciferase activity of tumor cells was determined. Viability was calculated by dividing siSCR normalized luciferase values of tumor cells cultured with FluT cells to respective medium-only values within each treatment condition (mean + SEM, n = 3).

(G) Lactic acid was added during coculture of FluT cells with PANC-1-LUC cells transfected with siPD-L1, and normalized viability was calculated. The experiment was performed once in triplicates; shown is the mean.

See also Figure S1.

investigated the effect of different NSAIDs on MCT transport activity in *Xenopus laevis* oocytes expressing either MCT1 or MCT4. Indeed, diclofenac inhibited transport activity of both MCT1 and MCT4, with a half maximal inhibitory concentration (IC_{50}) of 1.45 ± 0.04 μM for MCT1 and 0.14 ± 0.01 μM for MCT4. Thus, diclofenac is a potent MCT inhibitor and has an approximately 10-fold higher potency for MCT4 than for MCT1 (Figures 2A, 2B, S2A, and S2B). Furthermore, recovery of MCT4 transport activity was significantly reduced following washout of the drug compared to the recovery of MCT1 activity (Figures S2C and S2D), suggesting stronger binding of diclofenac to MCT4 than to MCT1. To clarify whether other NSAIDs are capable of blocking MCT activity, the effect of ketoprofen and lumiracoxib, which show structural similarity to diclofenac, as well as aspirin, were analyzed. Lumiracoxib also blocked MCT1 and MCT4 activity, however, at higher IC_{50} values

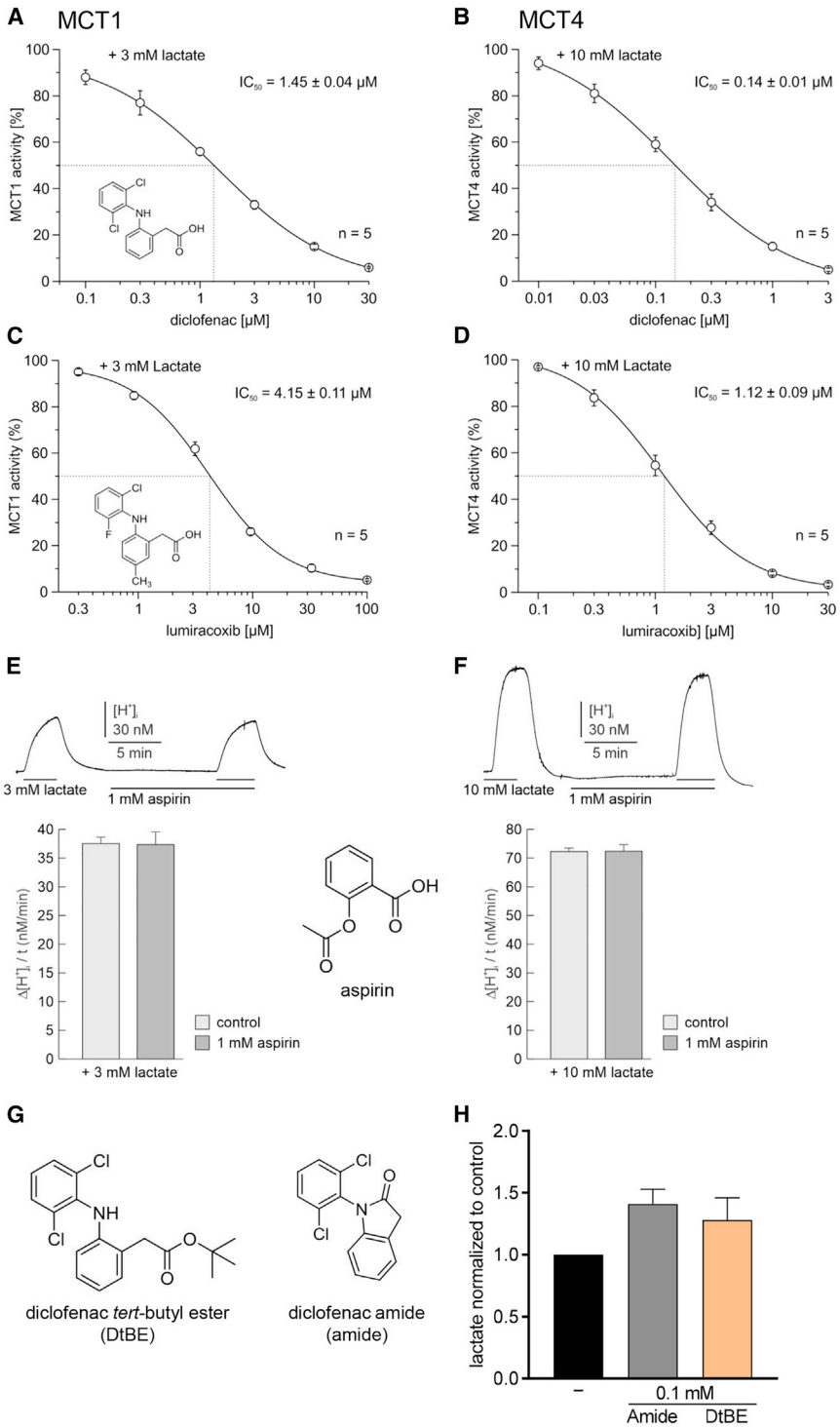

Figure 2. Diclofenac and Lumiracoxib Inhibit MCT1 and MCT4 Transport Activity

(A and B) Indicated concentrations of diclofenac were washed in for 10 min, and relative rate of change in $[H^+]_i$ ($\Delta[H^+]_i/\Delta t$) was determined as induced by application of (A) 3 mM lactate in *Xenopus* oocytes expressing MCT1 and (B) 10 mM lactate in oocytes expressing MCT4 (mean ± SEM, n = 5).

(C and D) Indicated concentrations of lumiracoxib were washed in for 10 min, and relative rate of change in $[H^+]_i$ ($\Delta[H^+]_i/\Delta t$) was determined as induced by application of (C) 3 mM lactate in oocytes expressing MCT1 and (D) by application of 10 mM lactate in oocytes expressing MCT4 (mean ± SEM, n = 5).

(E and F) Original recording showing change in intracellular H^+ concentration in oocytes during application of aspirin. $\Delta[H^+]i/\Delta t$ as induced by application of (E) 3 mM lactate in oocytes expressing MCT1 and (F) 10 mM lactate in oocytes expressing MCT4 before (light gray bar) and after (dark gray bar) 10 min wash in of 1 mM aspirin (mean ± SEM, n = 5).

(G and H) Impact of diclofenac derivatives (G) on lactate secretion (H) in a human melanoma cell line (MelIM). Lactate levels were normalized to control (mean+SEM, n = 3).

See also Figure S2.

(of 4.15 μM and 1.12 μM, respectively; Figures 2C and 2D). Ketoprofen inhibited MCT activity with an almost 100-fold higher IC_{50} than diclofenac (Figures S2E and S2F). Finally, aspirin had no impact on transport activity even at a concentration of 1.0 mM (Figures 2E and 2F). To clarify the importance of the monocarboxylate structure for MCT inhibition, we tested two structurally related compounds with blocked carboxyl groups (Figure 2G). Both diclofenac *tert*-butyl ester (DtBE) and diclofenac amid had no impact on lactate secretion (Figure 2H), indicating that the carboxyl group is essential for blocking MCT.

Lactate Lowering by Diclofenac Is Independent of Changes in Glycolysis-Associated Proteins and MCT Expression Profile

Diclofenac diminished lactate secretion of melanoma and pancreatic tumor cells. To investigate whether this is partially mediated by reducing the expression of the MCTs or suppression of glycolysis-related proteins, we analyzed MCT1, MCT4, LDHA, and LDHB protein levels after diclofenac treatment. No effects were observed in melanoma and pancreatic tumor cells (Figures 3A and 3B). To exclude an impact on PD-L1 and MHC-I expression, we performed flow cytometry analyses. We did not detect a suppressive effect of diclofenac on PD-L1 but saw a slightly upregulated MHC-I expression in melanoma cells (Figures 3C and 3D).

Next, the effect of diclofenac was compared to the clinically tested MCT1/2 inhibitor AZD3965 in tumor cell lines expressing

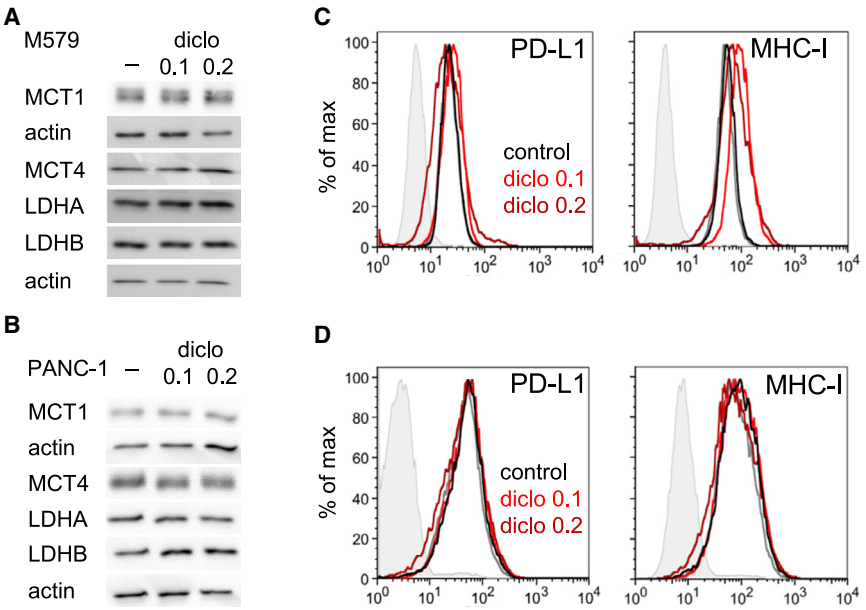

Figure 3. Effects of Diclofenac Are Independent of Changes in Glycolysis-Associated Proteins

(A and B) Expression of MCT1, MCT4, LDHA, and LDHB were analyzed in (A) M579 cells and (B) PANC-1 cells after 72 h of 0.1 or 0.2 mM diclofenac treatment. Protein expression was determined by western blot. One representative blot out of three independent experiments is shown.

(C and D) Surface expression of PD-L1 and MHC-I in (C) M579 and (D) PANC-1 cells was analyzed after 72 h of 0.1 and 0.2 mM diclofenac treatment by flow cytometry. One representative out of three independent experiments is shown.

See also Figure S3.

different MCT1 to MCT4 ratios. MCT1 was highly expressed in both cervix carcinoma cell lines investigated, but MCT4 was expressed at higher levels in OC-316 cells compared to IGROV-1 cells (Figure S3A). In accordance with the MCT expression profile, the MCT1/2 inhibitor AZD3965 reduced lactate secretion in IGROV-1 but not in OC-316 cells (Figure S3B). In contrast, diclofenac suppressed lactate secretion in both tumor cell lines (Figure S3B). The combination of diclofenac and AZD slightly augmented the reduction of lactate secretion in both cell lines (Figure S3B). To confirm on-target specificity of diclofenac and the MCT1/2 inhibitor, we assessed the effects of diclofenac versus AZD on human LS174T colorectal cancer cell clones expressing both MCT1 and MCT4 (wild type [WT]) in comparison to MCT1 ($MCT1^{-/-}$), $MCT4^{-/-}$ and MCT1/4 double knockout ($MCT1/4^{-/-}$). MCT expression was confirmed by western blot (Figure S3C). As expected, the MCT1/2 inhibitor strongly reduced lactate secretion only in $MCT4^{-/-}$ cells, whereas diclofenac diminished lactate efflux in the parental and the single-knockout clones but had no impact in $MCT1/4^{-/-}$ cells, which secreted very small amounts of lactate (Figure S3D).

MCT Inhibition Does Not Compromise T Cell Function *In Vitro*

Blocking MCT1/2 impairs glycolysis in lymphocytes (Murray et al., 2005), and diclofenac might affect glucose metabolism in T cells. The MCT expression was first assessed in quiescent and anti-CD3/CD28-stimulated human $CD8^+$ and $CD4^+$ T cells. Quiescent human T cells expressed very low levels of MCT1 and MCT4. Activation of T cells led to a marked and sustained upregulation of MCT1, whereas MCT4 induction was delayed but yet robust 6 days following stimulation (Figures 4A and S4A). In line with the MCT expression, the MCT1/2 inhibitor AZD3965 (AZD) reduced lactate secretion in stimulated human $CD8^+$ and $CD4^+$ T cells and 0.1 mM diclofenac had similar effects (Figures 4B and S4B). Treatment with 0.2 mM diclofenac led to a more profound decrease in lactate secretion, and this effect was only marginally intensified by the combined treatment with AZD (Figures 4B and S4B). As expected, reductions in lactate secretion correlated with a diminished glucose uptake (data not shown) and proliferation (Figures 4C and S4C). We also investigated the effect of lumiracoxib, as it displays the highest structural similarity to diclofenac and was capable of inhibiting both transporters in the low micromolar range. In line with higher IC_{50} values for both MCTs, lumiracoxib was capable of reducing lactate secretion and proliferation at a concentration of 0.2 mM (Figures 2B, 2C, S2B, and S2C). Nevertheless, viability was preserved under MCT inhibition (Figures 4D and S4D). Links between glucose metabolism and T cell function particularly regarding interferon gamma (IFNγ) production have been reported. Thus, we assessed whether reduced glycolytic activity triggered by MCT inhibition compromises human T cell function. The initial growth phase, the so-called "on-blast" formation, was not affected by treatment with diclofenac ± MCT1/2 inhibitors or lumiracoxib (data not shown). Analyses of cytokine production revealed that IFNγ (Figures 4E and S4E) and tumor necrosis factor (TNF) production (data not shown) were maintained in both T cell populations, even when diclofenac was combined with AZD-blocking MCT1, MCT2, and MCT4. Interleukin-2 (IL-2) production in $CD4^+$ T cells was unaffected by MCT inhibition (data not shown). Moreover, the expression of the activation-related molecules CD25, CD137, and PD-1 was unchanged in $CD8^+$ and $CD4^+$ T cells (Figures 4F and S4F).

Given the robust expression of both MCT1 and MCT4 after 6 days of expansion in $CD8^+$ and $CD4^+$ T cells (Figures 4G and S4G), we tested the impact of MCT inhibition on expanded and re-stimulated T cells. Lactate secretion was not affected by MCT1/2 inhibition (Figures 4H and S4H). These findings were confirmed by applying SR13800, another MCT1/2 inhibitor (data not shown) (Doherty et al., 2014). Diclofenac and lumiracoxib treatment reduced lactate secretion during re-stimulation in T cells after a 6-day expansion, although to a lower extent compared to freshly isolated and stimulated T cells (Figures 4H and S4H). Again, IFNγ secretion was preserved (Figures 4I and S4I). Similar to tumor cells,

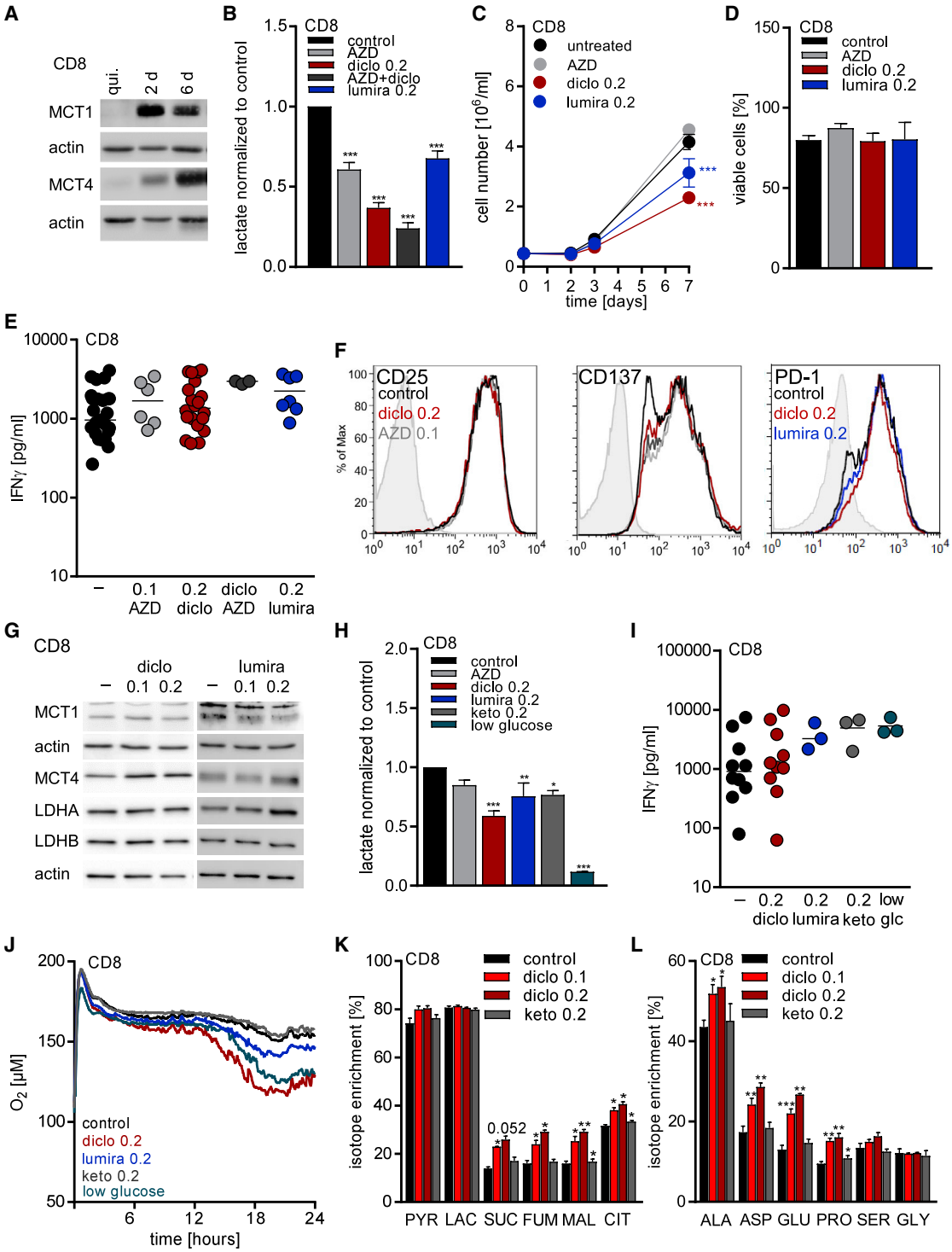

Figure 4. Diclofenac Treatment Preserves Effector Functions but Induces a Metabolic Shift from Glycolysis to Respiration in Human CD8$^+$ T Cells *In Vitro*

(A–E) CD8$^+$ T cells were freshly isolated and activated by anti-CD3/CD28 dynabeads.

(A) MCT1 and MCT4 expression in quiescent (qui.) and 2 day (2 d) and 6 day (6 d) stimulated CD8$^+$ T cells was determined by western blot. One representative blot is shown.

(B–F) MCT inhibitors were applied at the following concentrations: 0.1 μM AZD3965 (AZD), 0.2 mM diclofenac (diclo), or 0.2 mM lumiracoxib (lumira), and the combination of 0.2 mM diclofenac and 0.1 μM AZD3965.

(legend continued on next page)

the expression of glycolysis-related proteins was not affected (Figures 4G and S4G). The reduction in lactate secretion correlated with a diminished glucose uptake (data not shown), indicating profound changes in metabolism. Therefore, the impact of diclofenac on respiratory activity and glucose flux was analyzed in expanded T cells. Diclofenac treatment resulted in elevated cellular oxygen consumption (Figures 4J and S4J) and shifted glucose flux to tricarboxylic acid cycle (TCA) metabolites (Figures 4K and S4K). Moreover, glucose flux into amino acids related to TCA was increased (Figures 4L and S4L). In comparison to blocking glucose metabolism by MCT inhibition, we restricted the glucose level to 0.5 mM, resulting from serum addition. Similar to diclofenac and lumiracoxib, low glucose conditions resulted in decreased extracellular lactate levels (Figures 4H and S4H), preserved IFNγ secretion (Figures 4I and S4I), and elevated respiration (Figures 4J and S4J). Finally, we applied ketoprofen to control for possible COX-mediated effects. Ketoprofen exerted a slight impact on lactate secretion in $CD8^+$ T cells but not in $CD4^+$ T cells (Figures 4H and S4H) and did not affect IFNγ secretion, respiration, or glucose flux (Figures 4I–4L and S4I–S4L).

Polyclonal activation of T cells by anti-CD3/CD28 stimulation may not reflect responses observed following antigen presentation. Therefore, we assessed the effects of diclofenac on $CD4^+$ T cells stimulated with allogeneic dendritic cells. Diclofenac reduced glucose metabolism and proliferation, but T cell effector functions were preserved (Table S3).

As diclofenac might not completely block MCT1 and MCT4 activity in T cells, we assessed the impact of a complete inhibition of both transporters by using a *MCT4*$^{-/-}$ mouse model. MCT4 loss was confirmed by western blot of splenic T cells (Figures 5A and 5B). T cell populations were stimulated with anti-CD3/CD28 in the presence or absence of the MCT1/2 inhibitor SR13800. MCT1/2 inhibition reduced lactate secretion by about 70% in WT T cells and by 90% in *MCT4*$^{-/-}$ T cells (Figures 5C and 5D). MCT1/2 inhibition had no significant effect on IFNγ secretion in WT T cells and modestly reduced IFNγ secretion in *MCT4*$^{-/-}$ T cells (Figures 5E and 5F). Nonetheless, high levels of IFNγ were still detected following simultaneous blocking of MCT1, MCT2, and MCT4. The impact of diclofenac on IFNγ secretion was comparable to the combined blockade of MCT1, MCT2, and MCT4 (Figures 5G and 5H).

Finally, we tested whether *in vivo* administration of diclofenac affects T cell or NK cell levels in blood, spleen, or lymph nodes of healthy C57BL/6 mice. The percentage of $CD3^+$ T cells, $CD8^+$ T cells, and NK cells were not altered by diclofenac (Figures S5A–S5C). However, in tumor-bearing C57BL/6 mice, diclofenac treatment lowered the number of T cells in the spleen and in the blood (Figures S5D–S5E).

Targeting Tumor-Derived Lactic Acid Secretion Augments the Efficacy of Checkpoint Therapy

Lactic acid secretion of murine B16 melanoma cells promotes tumor growth in immunocompetent but not in immunodeficient mice (Brand et al., 2016). Both diclofenac and lumiracoxib reduced lactate secretion in B16 cells *in vitro* (Figure 6A) and elevated the pH in cell culture supernatants (Figures 6B and 6C). The immediate effect of diclofenac on pH further supports the notion that a reduction in proliferation (Figure 6D) is a secondary effect and not the cause for decreased extracellular lactate levels. Viability was only affected after 72 h at concentrations of 0.2 mM diclofenac or lumiracoxib (Figure 6E). Similar to human tumor cells and T cells, the expression of glycolysis-related proteins such as MCTs or LDH isoforms (Figure 6F) and PD-L1 or MHC expression (Figure 6G) was not altered by diclofenac. We analyzed whether diclofenac could also improve checkpoint blockade in a murine coculture model of SIY-specific T cells and SIY-expressing B16 tumor cells. Diclofenac clearly improved IFNγ secretion, especially in combination with anti-PD-1 treatment (Figure 6H). We, therefore, treated mice bearing B16 tumors with low dose diclofenac (7.5 mg/kg) alone or in

(B) Lactate levels were measured after 48 h in supernatants and normalized to control (one-way ANOVA, Dunnett's multiple comparisons test, * shows significant differences between control and treated cells, ***$p < 0.001$; mean + SEM, n = 13 for diclofenac, n = 7 for AZD3965, and n = 3 for the combination thereof, n = 6 for lumiracoxib-treated $CD8^+$ T cells).
(C) Proliferation of $CD8^+$ T cells was monitored over 7 days. Cell number was measured by the cell analyzing system (CASY; one-way ANOVA, Dunnett's multiple comparisons test, * shows significant differences between control and treated cells, ***$p < 0.001$; mean + SEM, n = 17 for control cells, n = 12 for diclofenac, n = 3 for AZD3965, and n = 10 for lumiracoxib-treated $CD8^+$ T cells).
(D) Viability of $CD8^+$ T cells was determined after 7 days (mean + SEM, n = 17 for control cells, n = 11 for diclofenac, n = 4 for AZD3965, and, n = 7 for lumiracoxib-treated $CD8^+$ T cells).
(E) IFNγ levels secreted by $CD8^+$ T cells were determined after 48 h in supernatants by ELISA (median, each symbol represents an independent donor).
(F) Representative flow cytometry blots show expression of CD25 and CD137 in freshly isolated and 48 h stimulated $CD8^+$ T cells. PD-1 expression was analyzed in 6 day expanded and for 48 h re-stimulated T cells. The signal on quiescent T cells as a negative control is shown for each antibody (filled gray).
(G–L) $CD8^+$ T cells were isolated, activated with anti-CD3/CD28 dynabeads, and expanded for 6 days. After 6 days, T cells were pooled and re-stimulated. Diclofenac was applied at 0.1 or 0.2 mM, AZD3965 at 0.1 μM, and lumiracoxib and ketoprofen at 0.2 mM. Low glucose (0.5 mM) was achieved by the usage of a glucose-free medium supplemented with 10% human serum.
(G) MCT1, MCT4, LDHA, and LDHB protein expression was determined by western blot after 72 h. One representative blot is shown.
(H) Lactate levels were measured in 48-h supernatants and normalized to control (one-way ANOVA, Dunnett's multiple comparisons test, * shows significant differences between control and treated cells, **$p < 0.01$, ***$p < 0.001$, mean + SEM, n = 9 for diclofenac, n = 3 for lumiracoxib, AZD, or low glucose).
(I) IFNγ levels in 48-h supernatants were determined by ELISA (median, each symbol represents an independent donor).
(J) Oxygen consumption was measured by the PreSens technology (mean of three independent donors).
(K and L) Glucose flux into (K) intermediates of glycolysis and TCA cycle or (L) amino acids was determined by mass spectrometry after 48 h (one-way ANOVA, Dunnett's multiple comparisons test, * shows significant differences between control and treated cells, *$p < 0.05$, **$p < 0.01$, ***$p < 0.001$, mean + SEM, n = 3). See also Figure S4.

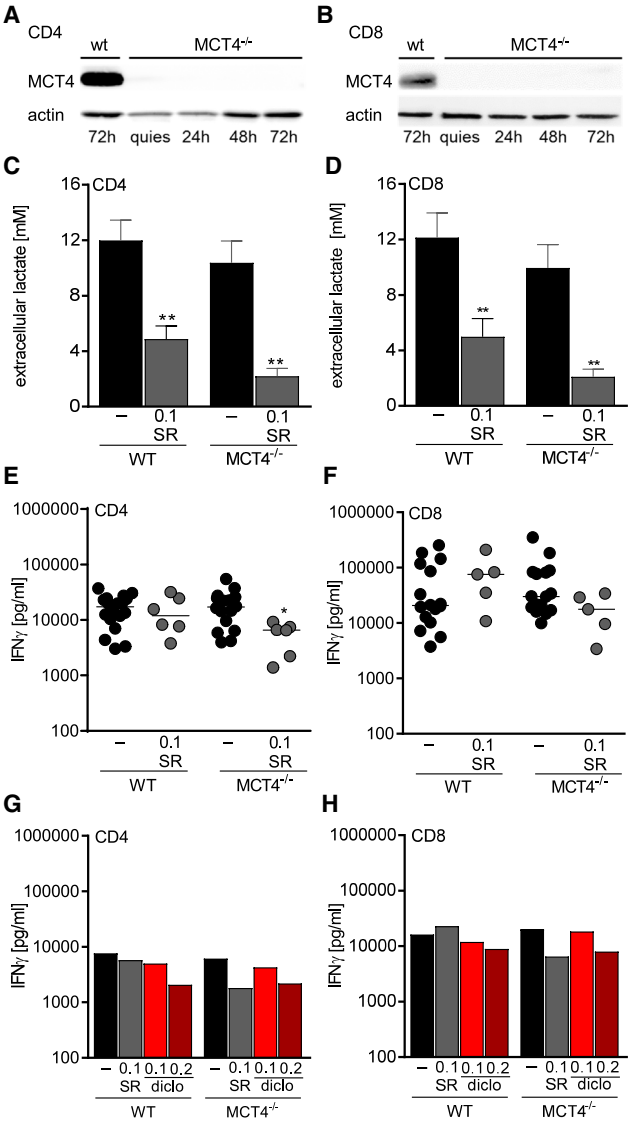

Figure 5. Combined MCT1/2 and MCT4 Blockade Only Moderately Affects T cell Function *In Vitro*

$CD4^+$ and $CD8^+$ T cell populations were isolated from spleens of WT and MCT4 knockout ($MCT4^{-/-}$) mice and activated with plate-bound anti-CD3 and soluble anti-CD28 antibodies.

(A and B) MCT4 expression in WT and $MCT4^{-/-}$ (A) $CD4^+$ and (B) $CD8^+$ T cells was determined by western blot at indicated time points. One representative western blot is shown.

(C–H) MCT inhibitors were applied at the following concentrations: 1 μM SR13800 (SR), 0.1, or 0.2 mM diclofenac.

(C and D) Lactate levels were measured in 48-h supernatants of SR-treated WT and $MCT4^{-/-}$ (C) $CD4^+$ and (D) $CD8^+$ T cells (Mann Whitney U test, *$p < 0.05$, mean + SEM, $n = 4$).

(E–H) IFNγ levels secreted by WT and $MCT4^{-/-}$ (E and G) $CD4^+$ or (F and H) $CD8^+$ T cells were determined by ELISA in supernatants of 48-h stimulated T cells (E and F, median, each symbol represents an individual mouse; G and H, mean of two independent experiments).

combination with anti-PD-1 antibodies. Diclofenac as well as anti-PD-1 alone had no effect, but the combination delayed tumor growth (Figure 6I). To improve tumor control, we applied diclofenac and lumiracoxib in higher concentrations (15 mg/kg) and administered anti-PD-1 and anti-CTLA-4 antibodies. In this setting, diclofenac alone partially controlled tumor growth and the combined anti-PD-1 and anti-CTLA-4 therapy was very effective. The combination of checkpoint therapy with diclofenac or lumiracoxib slightly improved tumor growth control (Figure 6J). As diclofenac and lumiracoxib elevated pH *in vitro* (Figures 6B and 6C), we measured the pH in B16 tumors. Both drugs elevated tumor pH by trend but showed a considerable variation suggesting a high metabolic heterogeneity (Figure 6K). To test whether normalization of tumor pH will result in a better response to checkpoint therapy, we used a genetic B16 $LDH^{-/-}$ knockout model characterized by a deletion of LDHA and LDHB (Ždralević et al., 2018). As expected from *in vitro* analyses (Figure 6B), intratumoral pH of B16 $LDH^{-/-}$ was comparable to blood pH in a range of 7.1 to 7.2 (Figure 6L). Furthermore, positron emission tomography (PET) analyses revealed significantly decreased glucose consumption in $LDH^{-/-}$ tumors (Figure 6M). In line with LDH-mediated lactate secretion and acidification as a resistance mechanism to immune checkpoint therapy, combined treatment with anti-PD-1 and anti-CTLA-4 antibodies resulted in a long-term growth control of B16 $LDH^{-/-}$ tumors (Figure 6N).

Finally, we investigated immune cell infiltration in B16 tumors. Upon checkpoint therapy, the number of tumor-infiltrating leukocytes ($CD45^+$) and T cell subpopulations ($CD3^+$, $CD3^+CD8^+$) increased in B16 WT and $LDH^{-/-}$ tumors (Figures S6A–S6C). T cell infiltration was even stronger in the direct comparison between B16 $LDH^{-/-}$ and WT tumors under checkpoint therapy ($p = 0.039$; Figure S6B). The combination of NSAIDs and checkpoint therapy did not further stimulate T cell infiltration; however, T cell activation in terms of IFNγ and IL-2 expression and PD-1 expression were higher in the presence of NSAIDs by trend, especially compared to checkpoint therapy (Figures 6O, S6D, and S6E). The highest number of $IFN\gamma^+$ T cells was found in checkpoint-treated B16 $LDH^{-/-}$ tumors (Figure 6O). Surprisingly, fewer NK cells were found after checkpoint therapy in B16 tumors. This effect was partially reverted by combination with diclofenac (Figure S6F). These data indicate that effective blockade of tumor glycolysis can augment immune cell infiltration and activation and, thereby, improve the response to checkpoint therapy. However, in the B16 model, diclofenac and lumiracoxib can only partially suppress tumor glycolysis.

To test whether the effect of diclofenac was manifested in other tumor models, the 4T1 model of triple-negative breast cancer was evaluated (Kaur et al., 2012). Aspirin was applied to assess the possible effects of COX inhibition. Diclofenac treatment reduced lactate secretion of 4T1 cells to a maximum of 40%, whereas aspirin had no effect *in vitro* (Figure 7A). In line with that result, diclofenac but not aspirin increased the pH in culture supernatants of 4T1 cells (Figure 7B). Diclofenac exerted an immediate impact on the extracellular pH that cannot be attributed to changes in proliferation. Thus, the reduction in proliferation and viability observed after 72 h is most likely the consequence of the reduced glycolytic activity (Figures 7C and 7D). In contrast to B16 tumor cells, diclofenac reduced LDHA and MCT1 expression in 4T1 cells (Figure 7E). MCT4 and LDHB were not expressed in 4T1 cells (Figure 7E). Furthermore, diclofenac partially reduced PD-L1 expression

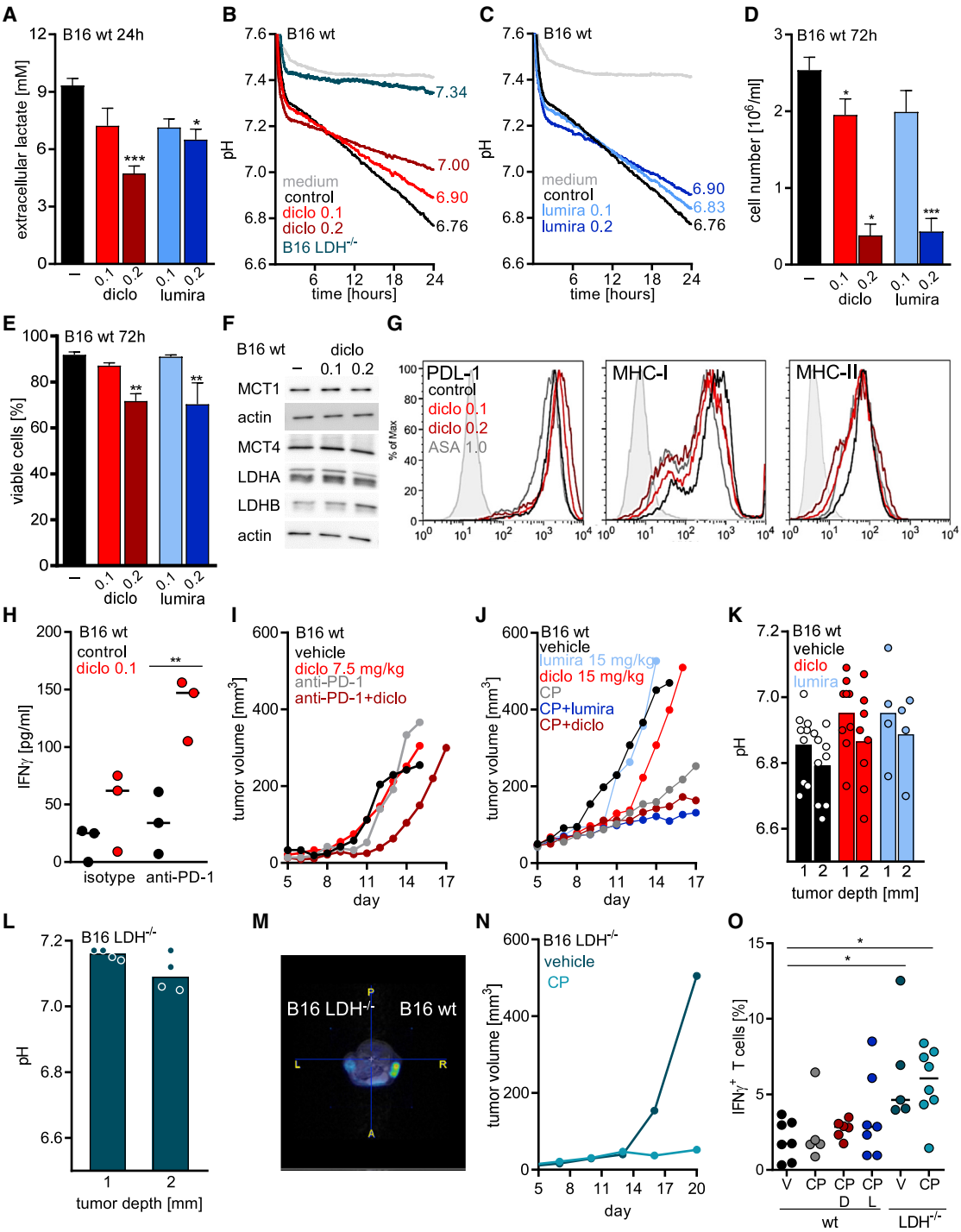

Figure 6. Modulating Glycolysis Augments the Efficacy of Checkpoint Inhibition in B16 Tumors

(A) Lactate levels were measured in supernatants of B16 WT cells in the presence or absence of 0.1 or 0.2 mM diclofenac as well as lumiracoxib (mean + SEM, n = 4, one-way ANOVA, Dunnett's multiple comparisons test, *p < 0.05, ***p < 0.001).

(B and C) Medium pH was monitored with the PreSens technology in supernatants of B16 WT cells under diclofenac treatment and B16 LDH$^{-/-}$ cells (B) or lumiracoxib-treated B16 WT cells (C) (mean, n = 3 for B16 WT cells, n = 2 for B16 LDH$^{-/-}$ cells).

(D) Cell number was analyzed using the CASY system (one-way ANOVA, Dunnett's multiple comparisons test, *p < 0.05, ***p < 0.001, mean+SEM, n = 3).

(E) Viability was determined (one-way ANOVA, Dunnett's multiple comparisons test, **p < 0.01, mean+SEM, n = 3, except for diclofenac 0.2 mM, where n = 4).

(F) MCT1, MCT4, LDHA, and LDHB protein expression was determined by western blot after 72 h. One representative blot is shown.

(G) Representative FACS blots showing expression of PD-L1, MHC-I, and MHC-II after 72 h of diclofenac treatment. Isotype staining is shown (filled gray).

(legend continued on next page)

and increased MHC-I and MHC-II expression of 4T1 cells (Figure 7F).

We injected 4T1 cells subcutaneously into BALB/c mice, and at day 6, mice were treated with diclofenac or aspirin (Figure 7G). Diclofenac delayed the growth of 4T1 tumors *in vivo*, whereas aspirin had only a slight impact (Figure 7G). Diclofenac also increased the intratumoral pH in this model (Figure 7H). However, the measurement was difficult due to a dense tumor structure. Therefore, these results have to be handled with caution. In contrast to the B16 model in C57BL/6 mice, immune cell infiltration ($CD45^+$ cells) was improved by diclofenac in 4T1 tumors ($p = 0.07$; Figures S7A and S7B), although the portion of $CD8^+$ T cells among $CD45^+$ cells was slightly decreased in 4T1 but not in B16 tumors (Figures S7C and S7D). Nevertheless, the number of activated $CD8^+$ T cells expressing CD25 was elevated by trend under diclofenac treatment in both models (Figures S7E and S7F). NK cell infiltration was consistently higher after diclofenac treatment in both models (Figures 7G and 7H). Furthermore, diclofenac elevated the number of $IFN\gamma^+$ NK cells but had no effect on IL-2 expression in 4T1 tumors (Figures 7I and 7J). Finally, among $CD45^+$ leukocytes, $CD11b^+$ myeloid cells represented the most frequent population and diclofenac had no impact on $CD11b^+$ cells (Figures S7I and S7J).

To investigate whether the observed changes in the immune composition could be translated into a better response to checkpoint therapy, we applied diclofenac or aspirin as a COX inhibitor control in combination with checkpoint therapy also in the 4T1 model. Checkpoint inhibitors were administered every third day for 1 week according to a previously developed protocol (Selby et al., 2016), and NSAIDs were administered for 14 days. In mice receiving checkpoint inhibitors, tumor growth was monitored for 30 days. Checkpoint blockade initially limited tumor growth in 11 of 14 mice, and yet, tumor outgrowth was observed after cessation of the drug in two more mice (Figure 7K). Aspirin had no positive impact on checkpoint blockade in this model (Figure 7L). Notably, in the cohort receiving diclofenac in combination with checkpoint blockade, tumor growth was inhibited in all mice even after cessation of checkpoint blockade as long as diclofenac was applied; only one tumor grew out after termination of diclofenac treatment (Figure 7M). However, some mice were found dead in the diclofenac treatment groups early on, the basis of which is unknown as no necropsies were performed in the first set of experiments. Due to these results, we investigated toxicity in the B16 (C57BL/6) model from all treatment groups. General histological analyses of lung, pancreas, liver, kidney, bone marrow, and stomach were performed in 42 tumor-bearing animals from all treatment groups. Signs of toxicity were detected in 2 out of 7 diclofenac-plus-checkpoint-treated mice and 1 of these mice had to be terminated. All other mice showed no signs of damage or inflammation in the examined organs (Figures S7K and S7L). Furthermore, we repeated the diclofenac treatment in the 4T1 model and no mice had to be terminated in the new set of experiments. Taken together, NSAIDs are known to induce gastrointestinal toxicity, which is in line with the observed local bowel inflammation in one mouse in the B16 model. This could be counteracted by the administration of proton-pump inhibitors as pantoprazole.

DISCUSSION

Targeting the glycolytic phenotype of tumor cells represents a promising approach from different perspectives. First, disabling glucose catabolism can compromise tumor growth and survival (Michelakis et al., 2008; Pedersen, 2012; Tennant et al., 2010). Second, restricting glycolytic activity of tumor cells reduces the secretion of lactate and acidification of the tumor milieu, which impairs the anti-tumor immune response of T and NK cells (Brand et al., 2016; Calcinotto et al., 2012; Müller et al., 2000). Accordingly, reducing intratumoral lactate levels and acidification promotes immunosurveillance and augments the efficacy of cancer immunotherapeutics (Brand et al., 2016; Calcinotto et al., 2012; Cascone et al., 2018; Long et al., 2018; Pilon-Thomas et al., 2016). In further support of this notion, Cascone et al. (2018) showed improved efficacy of adoptive T cell transfer in the presence of a glycolytic inhibitor. Our analyses of melanoma patients suggest a direct link between the response rate to checkpoint therapy and the glycolytic activity of tumors. In line with this, a negative correlation between overexpression of metabolic genes and response to anti-PD-1 therapy has been reported for renal cell carcinoma (Ascierto et al., 2016).

(H) B16.SIY WT cells and SIY-specific 2C $CD8^+$ T cells were cocultured for 24 h in the presence or absence of 0.1 mM diclofenac, anti-PD-1 antibody, or the respective isotype control. $IFN\gamma$ levels were determined in supernatants by ELISA (one-way ANOVA, Tukey's multiple comparisons test, $^{**}p < 0.01$, median, each symbol represents an independent experiment).
(I) 1.0×10^5 B16 WT cells were injected subcutaneously into the flank of C57BL/6 mice. Treatment was started when tumors were palpable. Diclofenac was applied intraperitoneally (i.p.) daily (7.5 mg/kg); anti-PD-1 antibody (20 mg/kg body weight) was administered i.p. every third day. Tumor volume was monitored over time (median, n = 7 for vehicle and anti-PD-1, n = 8 for diclofenac and diclofenac + anti-PD-1).
(J) 0.3×10^5 B16 WT cells were injected subcutaneously into the flank of C57BL/6 mice, and treatment was started when tumors were palpable. Diclofenac and lumiracoxib were applied i.p. daily (both 15 mg/kg); anti-PD-1 and anti-CTLA-4 (CP, both 10 mg/kg body weight) were administered i.p. Tumor volume was monitored over time (median, n = 9 for vehicle, n = 10 for checkpoint inhibitors combined with NSAIDs, n = 4 for diclofenac, n = 5 for lumiracoxib).
(K and L) Tumor pH was measured using a pH meter either at 1 or 2 mm depth (median, each symbol represents one individual tumor).
(K) pH of B16 WT tumors in vehicle-, diclofenac-, or lumiracoxib-treated mice was determined.
(L) pH in B16 $LDH^{-/-}$ tumors was measured.
(M) Glycolytic activity was determined *in vivo* by PET scan in B16 WT and $LDH^{-/-}$ tumors and injected into the right and left flank (shown is one representative image).
(N) 0.3×10^5 B16 $LDH^{-/-}$ cells were injected subcutaneously into the flank of C57BL/6 mice, and treatment was started when tumors were palpable. Anti-PD-1 and anti-CTLA-4 antibodies (CP, 10 mg/kg body weight) were administered i.p. every third day (median, n = 10).
(O) Percentage of $CD3^+IFN\gamma^+$ T cells in B16 WT or $LDH^{-/-}$ tumors under indicated conditions (V, vehicle;, CP, anti-PD-1 and anti-CTLA-4; D, diclofenac; L, lumiracoxib) was measured by flow cytometry (median, each symbol represents one individual tumor).
See also Figures S5, S6, and S7.

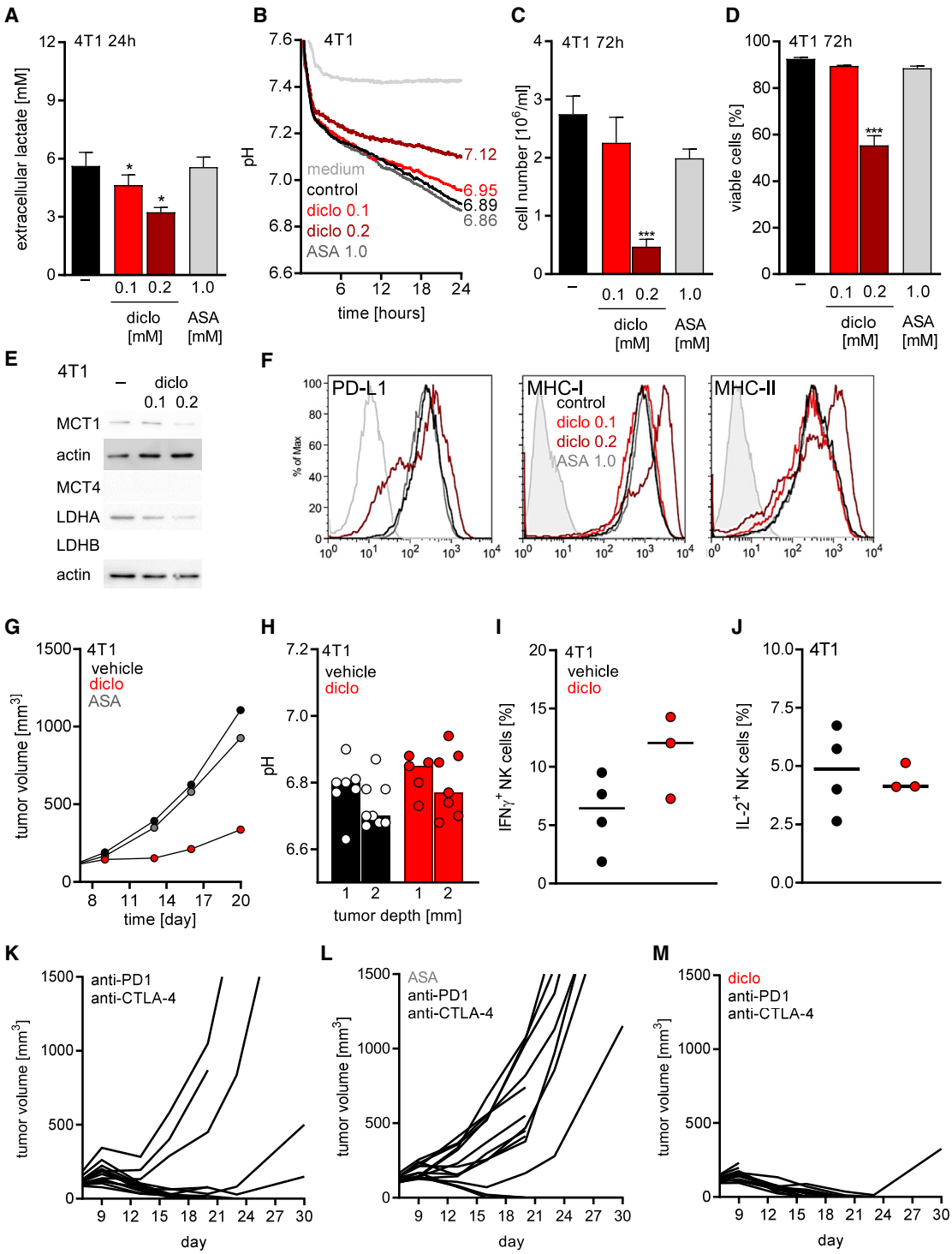

Figure 7. Diclofenac Augments the Efficacy of Checkpoint Inhibition in 4T1 Tumors

(A) Lactate levels were measured in supernatants of diclofenac- or aspirin-treated 4T1 cells (mean + SEM, n = 4, one-way ANOVA, Dunnet's multiple comparisons, *p < 0.05).

(B) Medium pH was monitored with the PreSens technology in supernatants of 4T1 cells under indicated conditions (mean of n = 3).

(C) Cell number was analyzed using the CASY system (one-way ANOVA, Dunnett's multiple comparisons test, ***p < 0.001, mean + SEM, n = 3).

(D) Viability was determined (one-way ANOVA, Dunnett's multiple comparisons test, ***p < 0.001, mean + SEM, n = 3).

(E) MCT1, MCT4, LDHA, and LDHB protein expression was determined by western blot after 72 h. One representative blot is shown.

(legend continued on next page)

MCTs are of crucial importance for glycolytic cells, as they remove lactate from the cells and, thereby, guarantee glycolytic flux, which is needed to supply metabolic intermediates for the highly anabolic tumor cells. The importance of MCTs in sustaining glycolysis, proliferation, and survival of tumor cells has been demonstrated in a variety of mouse models including melanoma and breast cancer (Baenke et al., 2015; Long et al., 2018; Morais-Santos et al., 2015). Elevated expression of MCT1 and MCT4 is also associated with poor prognosis in patients with breast cancer and melanoma (Baenke et al., 2015; Pinheiro et al., 2016). Thus, MCTs are attractive targets to limit glucose metabolism.

Currently, a limited number of clinically applicable drugs targeting MCTs are available. A MCT1/2 inhibitor is currently tested in a clinical trial (NCT01791595) as well as thalidomide, and its derivatives are feasible agents, as they destabilize the CD147-MCT1 complex (Eichner et al., 2016). Recently, Benjamin et al. (2018) showed that the anti-hypertensive drug syrosingopine is a dual MCT1 and MCT4 inhibitor. Another potential way to meet this need is the use of NSAIDs, which have been shown to impair lactate efflux and glucose metabolism (Emoto et al., 2002; Gottfried et al., 2013). In accordance with our studies, Sasaki et al. (2016) investigated the impact of diclofenac on MCT activity in oocytes expressing either MCT1 or MCT4. Here, we compared the impact of diclofenac, lumiracoxib, ketoprofen, and aspirin in *Xenopus* oocytes expressing either MCT1 or MCT4 and calculated their IC_{50} values. Among the tested NSAIDs, diclofenac had the lowest IC_{50} value, followed by lumiracoxib. In accordance with our oocyte experiments, diclofenac blocked MCT1 and MCT4 activity and lactate secretion in all tumor cell lines and primary T cells analyzed independently of their MCT1 and MCT4 expression profile and with an IC_{50} comparable to those reported for COX inhibition (Laneuville et al., 1994). In line with published data, the efficacy of MCT1/2 inhibition in our studies was limited by MCT4 expression (Baek et al., 2014; Doherty et al., 2014; Marchiq et al., 2015).

As glycolysis is accelerated in activated T cells, anti-glycolytic drugs might also impede their functions. Notably, although MCT inhibition by diclofenac or lumiracoxib lowered the glycolytic activity of T cells, effector functions and viability were preserved in our *in vitro* experiments. Indeed, even a complete block of MCT1, MCT2, and MCT4 did not block secretion of IFNγ in murine T cells; however, a reduction was observed. These findings are in accordance with *in vitro* studies showing that T cell functions are preserved under low glucose conditions, most likely due to their metabolic flexibility shifting from glycolysis to oxidative phosphorylation (Dziurla et al., 2010; Renner et al., 2015). In line with this, diclofenac shifted glucose flux into TCA metabolites and enhanced respiration. Metabolic flexibility was also observed *in vivo* in a murine mouse melanoma model. Here, tumor-infiltrating $CD8^+$ T cells subjected to hypoglycemia switched to fatty acid catabolism, resulting in preserved effector functions (Zhang et al., 2017).

Glycolysis has been demonstrated to be important for T cell effector functions for the following two reasons: (1) LDHA activity allows acetyl-coenzyme A (CoA) generation in the cytoplasm, which is necessary to enhance histone acetylation and, thereby, transcription of IFNγ (Peng et al., 2016); and (2) glycolytic activity hinders glyceraldehyde-3-phosphate dehydrogenase (GAPDH) binding to the 3′ UTR of IFNγ mRNA, thereby allowing translation (Chang et al., 2013). Targeting MCTs does not necessarily interfere with those two pathways, as glucose is still converted by GAPDH and LDHA to lactate, although to a lower extent.

Finally, diclofenac treatment of tumor cells augmented anti-PD-1-mediated T cell killing of melanoma cells *in vitro*. In line with this, diclofenac was capable of increasing the response to single anti-PD-1 blockade in B16 melanoma *in vivo* but only slightly and transiently improved dual-checkpoint therapy with anti-PD-1 and anti-CTLA-4. The same effect was observed for lumiracoxib. As already suggested by our *in vitro* results, NSAIDs did not negatively affect T cell infiltration and activation, as higher numbers of $PD\text{-}1^+$ $CD8^+$ T cells and IFNγ expressing $CD3^+$ T cells were detected under checkpoint therapy. Moreover, the number of NK cells was increased.

Both NSAIDs partially increased the intratumoral pH but not to the level detected in a genetic model displaying low glycolysis and PET activity due to LDHA and LDHB knockout. In this B16 $LDH^{-/-}$ model, checkpoint blockade controlled tumor growth and the number and activity of effector T cells was significantly increased compared to checkpoint-treated B16 WT tumors. Similar results were obtained with single-LDHA knockdown (Daneshmandi et al., 2019). These data suggest that PET activity might represent a feasible biomarker to stratify patients for checkpoint therapy. Patients with high glycolytic activity could benefit from a combination therapy including anti-glycolytic treatment plus checkpoint inhibition.

The combination of diclofenac with dual anti-PD-1 and anti-CTLA-4 therapy was even more effective in 4T1 tumors. Diclofenac alone impaired tumor growth and augmented the response to checkpoint inhibition. As observed in B16 WT tumors diclofenac treatment increased intratumoral pH and elevated the portion of NK cells. Furthermore, in 4T1 tumors, diclofenac treatment resulted in higher levels of tumor-infiltrating $CD45^+$ immune

(F) Representative FACS blots showing expression of PD-L1, MHC-I, and MHC-II after 72 h of treatment. Isotype staining is shown (filled gray).
(G–M) 1×10^6 4T1 cells were injected subcutaneously into BALB/c mice. NSAID and checkpoint inhibitor treatment was started on day 6. Diclofenac was applied i.p. twice a day (7.5 mg/kg) and aspirin (ASA) by addition to the drinking water at 600 μg/mL for 14 d; anti-PD-1 and anti-CTLA-4 antibodies were administered i.p. at a concentration of 10 mg/kg every 3–4 day for 1 week.
(G) Growth curves of vehicle-, diclofenac-, or aspirin-treated tumors are shown (median, n = 14).
(H) pH in 4T1 tumors was measured either at 1 or 2 mm depth (median, each symbol represents an individual tumor).
(I and J) Percentage of $IFN\gamma^+$ (I) and $IL\text{-}2^+$ (J) cells among NK cells derived from 4T1 tumors was determined by flow cytometry (median, each symbol represents one individual tumor).
(K–M) Individual growth curves of 4T1 tumors treated either with (K) anti-PD1 and anti-CTLA-4 antibodies, (L) aspirin combined with anti-PD1 and anti-CTLA-4 antibodies, or (M) diclofenac in combination with anti-PD-1 and anti-CTLA-4 antibodies are shown.
See also Figure S7.

cells *in vivo* and reduced MCT1 and LDHA protein levels and increased MHC-I and MHC-II surface expression *in vitro*. This could probably contribute to the better response to checkpoint therapy under diclofenac treatment. In contrast to a previous study (Zelenay et al., 2015), single treatment with aspirin did not alter tumor growth and failed to improve the efficacy of checkpoint blockade. This could reflect the different tumor models used, while NSAIDs might have tumor-specific effects, or the differences in treatment regimens. In our study, aspirin was administered after tumors were already established, whereas Zelenay et al. (2015) administered aspirin prior to injection of the tumor cells. As aspirin administration did not improve the efficacy of checkpoint therapy, COX inhibition might not be the primary cause for the positive impact of diclofenac on anti-PD1 and anti-CTLA-4 treatment.

Anti-tumor activity of diclofenac has been reported, and clinical trials were claimed (Pantziarka et al., 2016). We recently showed that topical administration of diclofenac in actinic keratosis, a pre-cancerous skin lesion, reduced lactate levels and increased IFNγ expression in responders (Singer et al., 2019). In line with this, the data of this study suggest that the main impact of diclofenac on checkpoint therapy is the upregulated IFNγ expression in T and NK cells.

Taken together, our results suggest that diclofenac supports an immune-cell-mediated anti-tumor response by reprogramming tumor glycolysis. Drugs lowering glycolytic activity by MCT or LDH inhibition represent a promising strategy to improve the response to checkpoint therapy. Based on our results, summarized in Table S4, diclofenac might be even more potent in the human system. Murine tumor cells seem to be less susceptible to lactate lowering by diclofenac, probably based on species-related structural differences in MCTs. As diclofenac is well tolerated, especially when combined with pantoprazole, our study provides a rationale for phase 1 trials combining diclofenac with immunotherapeutics (patent pending).

STAR★METHODS

Detailed methods are provided in the online version of this paper and include the following:

SUPPLEMENTAL INFORMATION

Supplemental Information can be found online at https://doi.org/10.1016/j.celrep.2019.08.068.

ACKNOWLEDGMENTS

We thank A. Peuker, G. Schoenhammer, M. Wehrstein, and E. Vollmer for their excellent technical support. We are grateful to R. Meier (PreSens, Regensburg, Germany) for intensive technical support. This study was supported by the KFO262 (Deutsche Forschungsgemeinschaft, DFG); the Regensburg Center of Interventional Immunology (RCI); II-ON Network; NIH/NCI R01 grant CA175094; Moffitt Cancer Center support grant P30 CA076292; Cortner-Couch Endowed Chair of Cancer Research; CRC1292 (Deutsche Forschungsgemeinschaft, DFG). The costs of publication of this article were defrayed in part by the payment of page charges. This article must, therefore, be hereby marked "advertisement" in accordance with 18 U.S.C. Section 1734 solely to indicate this fact.

AUTHOR CONTRIBUTIONS

Conception and design, K.R. and M.K; Development of methodology, W.R.R., I.M., K.D., S.A., and M.L; Acquisition of data, K.R., H.M.B., G.K., M.F., L.H., C. Bruss, A.-N.M., R.B., T. Bohn, S.P., M.M., K.E., S.A.L., O.K., E.A.R., S.F., L.A., C. Brummer, S.D., A.S., K.S., K.P., I.M., W.R.R., K.D., and M.S.; Analysis and interpretation of data, K.R., A.S., H.M.B., S.A.L., O.K., G.K., E.A.R., S.O., S.W., M.F., E.G., T. Bohn, T. Bopp, K.E., S.A., C.U.B., J.P., J.L.C., P.J.O., K.D., P.B., M.S., and M.K.; Writing, review and/or revision of the manuscript, K.R., H.M.B., E.G., T. Bopp, T.P., S.A., C.U.B., A.S., P.J.S., O.K., E.A.R., C. Bruss, S.O., W.H., J.P., J.L.C., M.S., P.B., and M.K.; Administrative, technical or material support, R.B., T. Bohn, M.K., K.R., W.R.R., J.L.C., I.M., and J.P.

DECLARATION OF INTERESTS

K.R., M.K., C.U.B., and E.A.R. report research grants from BMS.

Received: October 27, 2018
Revised: August 5, 2019
Accepted: August 22, 2019
Published: October 1, 2019

REFERENCES

Anderson, K.G., Stromnes, I.M., and Greenberg, P.D. (2017). Obstacles Posed by the Tumor Microenvironment to T cell Activity: A Case for Synergistic Therapies. Cancer Cell *31*, 311–325.

Andreesen, R., Scheibenbogen, C., Brugger, W., Krause, S., Meerpohl, H.G., Leser, H.G., Engler, H., and Löhr, G.W. (1990). Adoptive transfer of tumor cytotoxic macrophages generated in vitro from circulating blood monocytes: a new approach to cancer immunotherapy. Cancer Res. *50*, 7450–7456.

Ascierto, M.L., McMiller, T.L., Berger, A.E., Danilova, L., Anders, R.A., Netto, G.J., Xu, H., Pritchard, T.S., Fan, J., Cheadle, C., et al. (2016). The Intratumoral Balance between Metabolic and Immunologic Gene Expression Is Associated with Anti-PD-1 Response in Patients with Renal Cell Carcinoma. Cancer Immunol. Res. *4*, 726–733.

Baek, G., Tse, Y.F., Hu, Z., Cox, D., Buboltz, N., McCue, P., Yeo, C.J., White, M.A., DeBerardinis, R.J., Knudsen, E.S., and Witkiewicz, A.K. (2014). MCT4 defines a glycolytic subtype of pancreatic cancer with poor prognosis and unique metabolic dependencies. Cell Rep. *9*, 2233–2249.

Baenke, F., Dubuis, S., Brault, C., Weigelt, B., Dankworth, B., Griffiths, B., Jiang, M., Mackay, A., Saunders, B., Spencer-Dene, B., et al. (2015). Functional screening identifies MCT4 as a key regulator of breast cancer cell metabolism and survival. J. Pathol. *237*, 152–165.

Balar, A.V., and Weber, J.S. (2017). PD-1 and PD-L1 antibodies in cancer: current status and future directions. Cancer Immunol. Immunother. *66*, 551–564.

Becker, H.M. (2014). Transport of lactate: characterization of the transporters involved in transport at the plasma membrane by heterologous protein expression on Xenopus oocytes. In Neuromethods, J. Hirrlinger and H.S. Waagepetersen, eds. (Brain Energy Metabolism), pp. 25–43.

Becker, H.M., Bröer, S., and Deitmer, J.W. (2004). Facilitated lactate transport by MCT1 when coexpressed with the sodium bicarbonate cotransporter (NBC) in Xenopus oocytes. Biophys. J. *86*, 235–247.

Becker, H.M., Klier, M., and Deitmer, J.W. (2014). Carbonic anhydrases and their interplay with acid/base-coupled membrane transporters. Subcell. Biochem. *75*, 105–134.

Benjamin, D., Robay, D., Hindupur, S.K., Pohlmann, J., Colombi, M., El-Shemerly, M.Y., Maira, S.M., Moroni, C., Lane, H.A., and Hall, M.N. (2018). Dual Inhibition of the Lactate Transporters MCT1 and MCT4 Is Synthetic Lethal with Metformin due to NAD+ Depletion in Cancer Cells. Cell Rep. *25*, 3047–3058.e3044.

Bohn, T., Rapp, S., Luther, N., Klein, M., Bruehl, T.J., Kojima, N., Aranda Lopez, P., Hahlbrock, J., Muth, S., Endo, S., et al. (2018). Tumor immunoevasion via acidosis-dependent induction of regulatory tumor-associated macrophages. Nat. Immunol. *19*, 1319–1329.

Brand, A., Singer, K., Koehl, G.E., Kolitzus, M., Schoenhammer, G., Thiel, A., Matos, C., Bruss, C., Klobuch, S., Peter, K., et al. (2016). LDHA-Associated Lactic Acid Production Blunts Tumor Immunosurveillance by T and NK Cells. Cell Metab. *24*, 657–671.

Bröer, S., Bröer, A., Schneider, H.P., Stegen, C., Halestrap, A.P., and Deitmer, J.W. (1999). Characterization of the high-affinity monocarboxylate transporter MCT2 in Xenopus laevis oocytes. Biochem. J. *341*, 529–535.

Calcinotto, A., Filipazzi, P., Grioni, M., Iero, M., De Milito, A., Ricupito, A., Cova, A., Canese, R., Jachetti, E., Rossetti, M., et al. (2012). Modulation of microenvironment acidity reverses anergy in human and murine tumor-infiltrating T lymphocytes. Cancer Res. *72*, 2746–2756.

Cascone, T., McKenzie, J.A., Mbofung, R.M., Punt, S., Wang, Z., Xu, C., Williams, L.J., Wang, Z., Bristow, C.A., Carugo, A., et al. (2018). Increased Tumor Glycolysis Characterizes Immune Resistance to Adoptive T Cell Therapy. Cell Metab. *27*, 977–987.e974.

Chang, C.H., Curtis, J.D., Maggi, L.B., Jr., Faubert, B., Villarino, A.V., O'Sullivan, D., Huang, S.C., van der Windt, G.J., Blagih, J., Qiu, J., et al. (2013). Posttranscriptional control of T cell effector function by aerobic glycolysis. Cell *153*, 1239–1251.

Chang, C.H., Qiu, J., O'Sullivan, D., Buck, M.D., Noguchi, T., Curtis, J.D., Chen, Q., Gindin, M., Gubin, M.M., van der Windt, G.J., et al. (2015). Metabolic Competition in the Tumor Microenvironment Is a Driver of Cancer Progression. Cell *162*, 1229–1241.

Colegio, O.R., Chu, N.Q., Szabo, A.L., Chu, T., Rhebergen, A.M., Jairam, V., Cyrus, N., Brokowski, C.E., Eisenbarth, S.C., Phillips, G.M., et al. (2014). Functional polarization of tumour-associated macrophages by tumour-derived lactic acid. Nature *513*, 559–563.

Daneshmandi, S., Wegiel, B., and Seth, P. (2019). Blockade of Lactate Dehydrogenase-A (LDH-A) Improves Efficacy of Anti-Programmed Cell Death-1 (PD-1) Therapy in Melanoma. Cancers (Basel) *11*, E450.

Deitmer, J.W. (1991). Electrogenic sodium-dependent bicarbonate secretion by glial cells of the leech central nervous system. J. Gen. Physiol. *98*, 637–655.

Dimmer, K.S., Friedrich, B., Lang, F., Deitmer, J.W., and Bröer, S. (2000). The low-affinity monocarboxylate transporter MCT4 is adapted to the export of lactate in highly glycolytic cells. Biochem. J. *350*, 219–227.

Doherty, J.R., Yang, C., Scott, K.E., Cameron, M.D., Fallahi, M., Li, W., Hall, M.A., Amelio, A.L., Mishra, J.K., Li, F., et al. (2014). Blocking lactate export by inhibiting the Myc target MCT1 Disables glycolysis and glutathione synthesis. Cancer Res. *74*, 908–920.

Dziurla, R., Gaber, T., Fangradt, M., Hahne, M., Tripmacher, R., Kolar, P., Spies, C.M., Burmester, G.R., and Buttgereit, F. (2010). Effects of hypoxia and/or lack of glucose on cellular energy metabolism and cytokine production in stimulated human CD4+ T lymphocytes. Immunol. Lett. *131*, 97–105.

Eichner, R., Heider, M., Fernández-Sáiz, V., van Bebber, F., Garz, A.K., Lemeer, S., Rudelius, M., Targosz, B.S., Jacobs, L., Knorn, A.M., et al. (2016). Immunomodulatory drugs disrupt the cereblon-CD147-MCT1 axis to exert antitumor activity and teratogenicity. Nat. Med. *22*, 735–743.

Emoto, A., Ushigome, F., Koyabu, N., Kajiya, H., Okabe, K., Satoh, S., Tsukimori, K., Nakano, H., Ohtani, H., and Sawada, Y. (2002). H(+)-linked transport of salicylic acid, an NSAID, in the human trophoblast cell line BeWo. Am. J. Physiol. Cell Physiol. *282*, C1064–C1075.

Feist, M., Schwarzfischer, P., Heinrich, P., Sun, X., Kemper, J., von Bonin, F., Perez-Rubio, P., Taruttis, F., Rehberg, T., Dettmer, K., et al. (2018). Cooperative STAT/NF-κB signaling regulates lymphoma metabolic reprogramming and aberrant GOT2 expression. Nat. Commun. *9*, 1514.

Fischer, K., Hoffmann, P., Voelkl, S., Meidenbauer, N., Ammer, J., Edinger, M., Gottfried, E., Schwarz, S., Rothe, G., Hoves, S., et al. (2007). Inhibitory effect of tumor cell-derived lactic acid on human T cells. Blood *109*, 3812–3819.

Freemerman, A.J., Johnson, A.R., Sacks, G.N., Milner, J.J., Kirk, E.L., Troester, M.A., Macintyre, A.N., Goraksha-Hicks, P., Rathmell, J.C., and Makowski, L. (2014). Metabolic reprogramming of macrophages: glucose transporter 1 (GLUT1)-mediated glucose metabolism drives a proinflammatory phenotype. J. Biol. Chem. *289*, 7884–7896.

Gottfried, E., Lang, S.A., Renner, K., Bosserhoff, A., Gronwald, W., Rehli, M., Einhell, S., Gedig, I., Singer, K., Seilbeck, A., et al. (2013). New aspects of an old drug–diclofenac targets MYC and glucose metabolism in tumor cells. PLoS One *8*, e66987.

Gubser, P.M., Bantug, G.R., Razik, L., Fischer, M., Dimeloe, S., Hoenger, G., Durovic, B., Jauch, A., and Hess, C. (2013). Rapid effector function of memory CD8+ T cells requires an immediate-early glycolytic switch. Nat. Immunol. *14*, 1064–1072.

Heinrich, P., Kohler, C., Ellmann, L., Kuerner, P., Spang, R., Oefner, P.J., and Dettmer, K. (2018). Correcting for natural isotope abundance and tracer impurity in MS-, MS/MS- and high-resolution-multiple-tracer-data from stable isotope labeling experiments with IsoCorrectoR. Sci. Rep. *8*, 17910.

Heppt, M.V., Heinzerling, L., Kähler, K.C., Forschner, A., Kirchberger, M.C., Loquai, C., Meissner, M., Meier, F., Terheyden, P., Schell, B., et al. (2017). Prognostic factors and outcomes in metastatic uveal melanoma treated with programmed cell death-1 or combined PD-1/cytotoxic T-lymphocyte antigen-4 inhibition. Eur. J. Cancer *82*, 56–65.

Ho, P.C., Bihuniak, J.D., Macintyre, A.N., Staron, M., Liu, X., Amezquita, R., Tsui, Y.C., Cui, G., Micevic, G., Perales, J.C., et al. (2015).

Phosphoenolpyruvate Is a Metabolic Checkpoint of Anti-tumor T Cell Responses. Cell *162*, 1217–1228.

Jain, M., Nilsson, R., Sharma, S., Madhusudhan, N., Kitami, T., Souza, A.L., Kafri, R., Kirschner, M.W., Clish, C.B., and Mootha, V.K. (2012). Metabolite profiling identifies a key role for glycine in rapid cancer cell proliferation. Science *336*, 1040–1044.

Kaur, P., Nagaraja, G.M., Zheng, H., Gizachew, D., Galukande, M., Krishnan, S., and Asea, A. (2012). A mouse model for triple-negative breast cancer tumor-initiating cells (TNBC-TICs) exhibits similar aggressive phenotype to the human disease. BMC Cancer *12*, 120.

Kelderman, S., Heemskerk, B., van Tinteren, H., van den Brom, R.R., Hospers, G.A., van den Eertwegh, A.J., Kapiteijn, E.W., de Groot, J.W., Soetekouw, P., Jansen, R.L., et al. (2014). Lactate dehydrogenase as a selection criterion for ipilimumab treatment in metastatic melanoma. Cancer Immunol. Immunother. *63*, 449–458.

Kelly, B., and O'Neill, L.A. (2015). Metabolic reprogramming in macrophages and dendritic cells in innate immunity. Cell Res. *25*, 771–784.

Laneuville, O., Breuer, D.K., Dewitt, D.L., Hla, T., Funk, C.D., and Smith, W.L. (1994). Differential inhibition of human prostaglandin endoperoxide H synthases-1 and -2 by nonsteroidal anti-inflammatory drugs. J. Pharmacol. Exp. Ther. *271*, 927–934.

Le Floch, R., Chiche, J., Marchiq, I., Naiken, T., Ilc, K., Murray, C.M., Critchlow, S.E., Roux, D., Simon, M.P., and Pouysségur, J. (2011). CD147 subunit of lactate/H+ symporters MCT1 and hypoxia-inducible MCT4 is critical for energetics and growth of glycolytic tumors. Proc. Natl. Acad. Sci. USA *108*, 16663–16668.

Loftus, R.M., Assmann, N., Kedia-Mehta, N., O'Brien, K.L., Garcia, A., Gillespie, C., Hukelmann, J.L., Oefner, P.J., Lamond, A.I., Gardiner, C.M., et al. (2018). Amino acid-dependent cMyc expression is essential for NK cell metabolic and functional responses in mice. Nat. Commun. *9*, 2341.

Long, Y., Gao, Z., Hu, X., Xiang, F., Wu, Z., Zhang, J., Han, X., Yin, L., Qin, J., Lan, L., et al. (2018). Downregulation of MCT4 for lactate exchange promotes the cytotoxicity of NK cells in breast carcinoma. Cancer Med. *7*, 4690–4700.

Machlenkin, A., Uzana, R., Frankenburg, S., Eisenberg, G., Eisenbach, L., Pitcovski, J., Gorodetsky, R., Nissan, A., Peretz, T., and Lotem, M. (2008). Capture of tumor cell membranes by trogocytosis facilitates detection and isolation of tumor-specific functional CTLs. Cancer Res. *68*, 2006–2013.

Macintyre, A.N., Gerriets, V.A., Nichols, A.G., Michalek, R.D., Rudolph, M.C., Deoliveira, D., Anderson, S.M., Abel, E.D., Chen, B.J., Hale, L.P., and Rathmell, J.C. (2014). The glucose transporter Glut1 is selectively essential for CD4 T cell activation and effector function. Cell Metab. *20*, 61–72.

Marchiq, I., Le Floch, R., Roux, D., Simon, M.P., and Pouyssegur, J. (2015). Genetic disruption of lactate/H+ symporters (MCTs) and their subunit CD147/BASIGIN sensitizes glycolytic tumor cells to phenformin. Cancer Res. *75*, 171–180.

Michelakis, E.D., Webster, L., and Mackey, J.R. (2008). Dichloroacetate (DCA) as a potential metabolic-targeting therapy for cancer. Br. J. Cancer *99*, 989–994.

Migali, C., Milano, M., Trapani, D., Criscitiello, C., Esposito, A., Locatelli, M., Minchella, I., and Curigliano, G. (2016). Strategies to modulate the immune system in breast cancer: checkpoint inhibitors and beyond. Ther. Adv. Med. Oncol. *8*, 360–374.

Morais-Santos, F., Granja, S., Miranda-Gonçalves, V., Moreira, A.H., Queirós, S., Vilaça, J.L., Schmitt, F.C., Longatto-Filho, A., Paredes, J., Baltazar, F., and Pinheiro, C. (2015). Targeting lactate transport suppresses in vivo breast tumour growth. Oncotarget *6*, 19177–19189.

Müller, B., Fischer, B., and Kreutz, W. (2000). An acidic microenvironment impairs the generation of non-major histocompatibility complex-restricted killer cells. Immunology *99*, 375–384.

Murray, C.M., Hutchinson, R., Bantick, J.R., Belfield, G.P., Benjamin, A.D., Brazma, D., Bundick, R.V., Cook, I.D., Craggs, R.I., Edwards, S., et al. (2005). Monocarboxylate transporter MCT1 is a target for immunosuppression. Nat. Chem. Biol. *1*, 371–376.

Ottensmeier, C.H., Perry, K.L., Harden, E.L., Stasakova, J., Jenei, V., Fleming, J., Wood, O., Woo, J., Woelk, C.H., Thomas, G.J., and Thirdborough, S.M. (2016). Upregulated Glucose Metabolism Correlates Inversely with CD8+ T-cell Infiltration and Survival in Squamous Cell Carcinoma. Cancer Res. *76*, 4136–4148.

Pantziarka, P., Sukhatme, V., Bouche, G., Meheus, L., and Sukhatme, V.P. (2016). Repurposing Drugs in Oncology (ReDO)-diclofenac as an anti-cancer agent. Ecancermedicalscience *10*, 610.

Pedersen, P.L. (2012). 3-Bromopyruvate (3BP) a fast acting, promising, powerful, specific, and effective "small molecule" anti-cancer agent taken from labside to bedside: introduction to a special issue. J. Bioenerg. Biomembr. *44*, 1–6.

Peng, M., Yin, N., Chhangawala, S., Xu, K., Leslie, C.S., and Li, M.O. (2016). Aerobic glycolysis promotes T helper 1 cell differentiation through an epigenetic mechanism. Science *354*, 481–484.

Pilon-Thomas, S., Kodumudi, K.N., El-Kenawi, A.E., Russell, S., Weber, A.M., Luddy, K., Damaghi, M., Wojtkowiak, J.W., Mulé, J.J., Ibrahim-Hashim, A., and Gillies, R.J. (2016). Neutralization of Tumor Acidity Improves Antitumor Responses to Immunotherapy. Cancer Res. *76*, 1381–1390.

Pinheiro, C., Miranda-Gonçalves, V., Longatto-Filho, A., Vicente, A.L., Berardinelli, G.N., Scapulatempo-Neto, C., Costa, R.F., Viana, C.R., Reis, R.M., Baltazar, F., and Vazquez, V.L. (2016). The metabolic microenvironment of melanomas: Prognostic value of MCT1 and MCT4. Cell Cycle *15*, 1462–1470.

Qin, C., and Davies, H.M. (2013). Rh2(R-TPCP)4-catalyzed enantioselective [3+2]-cycloaddition between nitrones and vinyldiazoacetates. J. Am. Chem. Soc. *135*, 14516–14519.

Renner, K., Geiselhöringer, A.L., Fante, M., Bruss, C., Färber, S., Schönhammer, G., Peter, K., Singer, K., Andreesen, R., Hoffmann, P., et al. (2015). Metabolic plasticity of human T cells: Preserved cytokine production under glucose deprivation or mitochondrial restriction, but 2-deoxy-glucose affects effector functions. Eur. J. Immunol. *45*, 2504–2516.

Sasaki, S., Futagi, Y., Ideno, M., Kobayashi, M., Narumi, K., Furugen, A., and Iseki, K. (2016). Effect of diclofenac on SLC16A3/MCT4 by the Caco-2 cell line. Drug Metab. Pharmacokinet. *31*, 218–223.

Schröder, M.S., Culhane, A.C., Quackenbush, J., and Haibe-Kains, B. (2011). survcomp: an R/Bioconductor package for performance assessment and comparison of survival models. Bioinformatics *27*, 3206–3208.

Selby, M.J., Engelhardt, J.J., Johnston, R.J., Lu, L.S., Han, M., Thudium, K., Yao, D., Quigley, M., Valle, J., Wang, C., et al. (2016). Preclinical Development of Ipilimumab and Nivolumab Combination Immunotherapy: Mouse Tumor Models, In Vitro Functional Studies, and Cynomolgus Macaque Toxicology. PLoS One *11*, e0161779.

Sharma, P., Hu-Lieskovan, S., Wargo, J.A., and Ribas, A. (2017). Primary, Adaptive, and Acquired Resistance to Cancer Immunotherapy. Cell *168*, 707–723.

Singer, K., Kastenberger, M., Gottfried, E., Hammerschmied, C.G., Büttner, M., Aigner, M., Seliger, B., Walter, B., Schlösser, H., Hartmann, A., et al. (2011). Warburg phenotype in renal cell carcinoma: high expression of glucose-transporter 1 (GLUT-1) correlates with low CD8(+) T-cell infiltration in the tumor. Int. J. Cancer *128*, 2085–2095.

Singer, K., Dettmer, K., Unger, P., Schönhammer, G., Renner, K., Peter, K., Siska, P.J., Berneburg, M., Herr, W., Oefner, P.J., et al. (2019). Topical Diclofenac Reprograms Metabolism and Immune Cell Infiltration in Actinic Keratosis. Front. Oncol. *9*, 605.

Tennant, D.A., Durán, R.V., and Gottlieb, E. (2010). Targeting metabolic transformation for cancer therapy. Nat. Rev. Cancer *10*, 267–277.

van der Windt, G.J., and Pearce, E.L. (2012). Metabolic switching and fuel choice during T-cell differentiation and memory development. Immunol. Rev. *249*, 27–42.

Wen, X., Ding, Y., Li, J., Zhao, J., Peng, R., Li, D., Zhu, B., Wang, Y., Zhang, X., and Zhang, X. (2017). The experience of immune checkpoint inhibitors in

Chinese patients with metastatic melanoma: a retrospective case series. Cancer Immunol. Immunother. *66*, 1153–1162.

Ždralević, M., Brand, A., Di Ianni, L., Dettmer, K., Reinders, J., Singer, K., Peter, K., Schnell, A., Bruss, C., Decking, S.M., et al. (2018). Double genetic disruption of lactate dehydrogenases A and B is required to ablate the "Warburg effect" restricting tumor growth to oxidative metabolism. J. Biol. Chem. *293*, 15947–15961.

Zelenay, S., van der Veen, A.G., Böttcher, J.P., Snelgrove, K.J., Rogers, N., Acton, S.E., Chakravarty, P., Girotti, M.R., Marais, R., Quezada, S.A., et al. (2015). Cyclooxygenase-Dependent Tumor Growth through Evasion of Immunity. Cell *162*, 1257–1270.

Zhang, Y., Kurupati, R., Liu, L., Zhou, X.Y., Zhang, G., Hudaihed, A., Filisio, F., Giles-Davis, W., Xu, X., Karakousis, G.C., et al. (2017). Enhancing CD8(+) T Cell Fatty Acid Catabolism within a Metabolically Challenging Tumor Microenvironment Increases the Efficacy of Melanoma Immunotherapy. Cancer Cell *32*, 377–391.e379.

Zhao, X., and Subramanian, S. (2017). Intrinsic Resistance of Solid Tumors to Immune Checkpoint Blockade Therapy. Cancer Res. *77*, 817–822.

STAR★METHODS

KEY RESOURCES TABLE

REAGENT or RESOURCE	SOURCE	IDENTIFIER
Antibodies		
Anti-Human CD4 (clone RPA-T4)	BD Biosciences	Cat# 561844, RRID:AB_11153855
Anti-Human CD8 (clone SK1)	BioLegend	Cat# 344712, RRID:AB_2044008
Anti-Human CD25 (clone M-A251)	BD Biosciences	Cat# 557741, RRID:AB_396847
Anti-Human CD137 (clone 4B4-1)	Thermo Fisher Scientific	Cat# 12-1379-42, RRID:AB_127208
Anti-Human CD152 (CTLA-4, clone BNI3)	BD Biosciences	Cat# 560939, RRID:AB_10563068
Anti-Human CD279 (PD-1, clone EH12.2H7)	BioLegend	Cat# 329908, RRID:AB_940475
Anti-Human CD274 (PD-L1, clone 29E.2A3)	BioLegend	Cat# 329708, RRID:AB_940360
Anti-Human HLA-ABC (clone G46-2.6)	BD Biosciences	Cat# 555554, RRID:AB_395937
Annexin-V	BD Biosciences	Cat# 556419, RRID:AB_2665412
7-AAD	BD Biosciences	Cat# 559925
Anti-Mouse CD3e (Clone 145-2C11)	Thermo Fisher Scientific	Cat# 11-0031-85, RRID:AB_464883
Anti-Mouse CD3e (clone 145-2C11)	BD Biosciences	Cat# 566494, RRID:AB_2744393
Anti-Mouse CD4 (clone RM4-5)	Thermo Fisher Scientific	Cat# 17-0042-82, RRID:AB_469323
Anti-Mouse CD4 (clone RM4-5)	BioLegend	Cat# 100528, RRID:AB_312729
Anti-Mouse CD4 (clone RM4-5)	BioLegend	Cat# 100559, RRID:AB_2562608
Anti-Mouse CD8a (clone 53-6.7)	BD Biosciences	Cat# 553036, RRID:AB_394573
Anti-Mouse CD8a (clone REA601)	Miltenyi Biotec	Cat# 130-109-247, RRID:AB_2659492
Anti-Mouse CD45 (clone 30-F11)	BD Biosciences	Cat# 553081, RRID:AB_394611
Anti-Mouse CD45 (clone REA737)	Miltenyi Biotec	Cat# 130-110-658, RRID:AB_2658217
Anti-Mouse CD274 (PD-L1, clone 10F.9G2)	BioLegend	Cat# 124311, RRID:AB_10612935
Anti-Mouse CD335 (NKp46, clone 29A1.4)	BioLegend	Cat# 137608, RRID:AB_10612758
Anti-Mouse NK1.1 (clone PK136)	BioLegend	Cat# 108741, RRID:AB_2562561
Anti-Mouse NK1.1 (clone PK136)	Thermo Fisher Scientific	Cat# 17-5941-82, RRID:AB_469479
Anti-Mouse IFNγ (clone XMG1.2)	BioLegend	Cat# 505810, RRID:AB_315404
Anti-Mouse I-Ab (clone AF6-120.1)	BioLegend	Cat# 116405, RRID:AB_313724
Anti-Mouse I-A/I-E (clone M5/114.15.2)	BioLegend	Cat# 107607, RRID:AB_313322
Anti-Mouse H-2Kb (clone AF6-88.5)	BD Biosciences	Cat# 553570, RRID:AB_394928
Anti-Mouse H-2Dd (clone 34-2-12)	BioLegend	Cat# 110607, RRID:AB_313488
Anti-MCT1 Monoclonal Antibody (P14612)	Thermo Fisher Scientific	Cat# MA5-18288, RRID:AB_2539662
Anti-MCT1 Monoclonal Antibody (H-1)	Santa Cruz Biotechnology	Cat# sc-365501, RRID:AB_10841766
Anti-MCT4 Polyclonal Antibody (H-90)	Santa Cruz Biotechnology	Cat# sc-50329, RRID:AB_2189333
Anti-GLUT1 Polyclonal Antibody	Abcam	Cat# ab652, RRID:AB_305540
Anti-LDHA Polyclonal Antibody	Cell Signaling Technology	Cat# 2012, RRID:AB_2137173
Anti-LDHB Monoclonal Antibody (431.1)	Santa Cruz Biotechnology	Cat# sc-100775, RRID:AB_1124720
Anti-Actin Polyclonal Antibody	Sigma-Aldrich	Cat# A2066, RRID:AB_476693
Goat Anti- Rabbit Immunoglobulins antibody (polyclonal)	Agilent (former Dako)	Cat# P0448, RRID:AB_2617138
Goat Anti- Mouse Immunoglobulins antibody (polyclonal)	Agilent (former Dako)	Cat# P0447, RRID:AB_2617137
Anti-CD3e (unconjugated, clone 145-2C11)	BD Biosciences	Cat# 553057, RRID:AB_394590
Anti-CD28 (unconjugated, clone 37.51)	BD Biosciences	Cat# 553294, RRID:AB_394763

(*Continued on next page*)

Continued

REAGENT or RESOURCE	SOURCE	IDENTIFIER
LEAF Purified Rat IgG2b, kappa Isotype Ctrl antibody (coculture, clone RTK4530)	BioLegend	Cat# 400622, RRID:AB_326564
LEAF Purified anti-Mouse CD279 (PD-1) antibody (coculture, clone 29F.1A12)	BioLegend	Cat# 135204, RRID:AB_1877087
anti-PD-1 antibody (*in vivo*, clone RMP1-14)	Leinco Technologies, Inc.	Cat# P372, RRID:AB_2749820
anti-PD-1 antibody (*in vivo*, clone 29F.1A12)	Bio X Cell	Cat# BE0273 RRID:AB_2687796
anti-PD-1 antibody (*in vivo*, clone 4H2)	BMS	N/A
anti-CTLA-4 (CD152) antibody (*in vivo*, clone 9D9)	Bio X Cell	Cat# BE0164, RRID:AB_10949609
anti-CTLA-4 (CD152) antibody (*in vivo*, clone 9D9)	BMS	N/A
Bacterial and Virus Strains		
Biological Samples		
Melanoma patient material	the Netherlands Cancer Institute	
Chemicals, Peptides, and Recombinant Proteins		
FcR Blocking Reagent, mouse	Miltenyi Biotec	Cat# 130-092-575
Zombie NIR Fixable Viability Kit	BioLegend	Cat# 423106
Lipofectamine RNAiMAX Transfection Reagent	Thermo Fisher Scientific	Cat# 13778030
Dynabeads Human T-Activator CD3/CD28	Thermo Fisher Scientific	Cat# 11132D
Recombinant Murine IFNγ	PeproTech	*Cat# 315-05*
Recombinant Human IL-2	PeproTech	*200-02*
Recombinant Human IL-4	PeproTech	*200-04*
Recombinant Human IL-15	R&D systems	*247-ILB-005/CF*
Recombinant Human GM-CSF	PeproTech	*300-03*
Protein Transport Inhibitor (Containing Monensin)	BD Biosciences	Cat# 554724
Intracellular Fixation and Permeabilization Buffer Set	Thermo Fisher Scientific	Cat# 88-8824-00
RIPA Buffer	Sigma-Aldrich	Cat# R0278
Diclofenac	Sigma-Aldrich	Cat# D6899
Lumiracoxib	Selleckchem	Cat# S2903
Acetyl salicylic acid	Fagron	Cat# 701627-0003
Ketoprofen	Sigma-Aldrich	Cat# 471909
AZD3965	Tocris	Cat# 4960
SR13800	gift from Prof. Cleveland	N/A
LPS	ENZO	Cat# ALX-581-009-L002
^{13}C Glucose (U-13C6)	Cambridge Isotope Laboratories	Cat# 110187-42-3
Flu peptide (GILGFVFTL)	ProImmune	P007-0A-E
Critical Commercial Assays		
RNeasy Mini Kit	QUIAGEN	Cat# 74104
AllPrep DNA/RNA Mini Kit	QUIAGEN	Cat# 80204
CD4+ isolation kit, human	Miltenyi Biotec	Cat# 130-045-101
CD8+ isolation kit, human	Miltenyi Biotec	Cat# 130-045-201
CD4+ isolation kit, murine	Miltenyi Biotec	Cat# 130-049-201
CD8+ isolation kit, murine	Miltenyi Biotec	Cat# 130-104-075
Glucose (HK) Assay Kit	Sigma-Aldrich	Cat# GAHK20-1KT
Human IFNγ DuoSet ELISA	R&D Systems	Cat# DY285
Human TNF DuoSet ELISA	R&D Systems	Cat# DY210

(*Continued on next page*)

Continued

REAGENT or RESOURCE	SOURCE	IDENTIFIER
Human IL-2 DuoSet ELISA	R&D Systems	Cat# DY202
Mouse IFNγ DuoSet ELISA	R&D Systems	Cat# DY485
Experimental Models: Cell Lines		
M579-LUC (human)	Machlenkin et al., 2008	N/A
OC316 (human)	Gift from Prof. Dr. Mueller-Klieser	N/A
IGROV-1 (human)	Gift from Prof. Dr. Mueller-Klieser	N/A
LS174T wt (human)	Marchiq et al., 2015	N/A
LS174T MCT$^{-/-}$ (human)	Marchiq et al., 2015	N/A
PANC-1 (human)	ATCC	Cat#CRL-1469
4T1 (murine)	Gift from Prof. Dr. Balkwill	N/A
B16.SIY wt (murine)	Brand et al., 2016	N/A
B16.SIY LDH$^{-/-}$ (murine)	Ždralević et al., 2018	N/A
MelIM	Gift from Prof. Dr. Judith Johnson	N/A
Experimental Models: Organisms/Strains		
Mouse: C57BL/6N	Charles River	strain code 027
Mouse: C57BL/6J	Charles River	strain code 632
Mouse: C57BL/6J MCT4$^{-/-}$	In cooperation with Prof. Dr. Cleveland	N/A
Mouse: 2C/Rag2−/−	bred in-house	N/A
Mouse: BALB/c	bred in-house	N/A
Frog: *Xenopus laevis*	*Xenopus* Express	Cat# IMP XL FM
Oligonucleotides		
Hs_CD274_1_SG QuantiTect Primer Assay	Quiagen	Cat# QT00082775
beta actin for primer AGAAAATCTGGCACCACACC	Sigma-Aldrich	N/A
beta actin rev primer GGGGTGTTGAAGGTCTCAAA	Sigma-Aldrich	N/A
Software and Algorithms		
FlowJo	Tree Star Inc	https://www.flowjo.com/
GraphPad Prism software	GraphPad Software	https://www.graphpad.com/scientific-software/prism/
PreSens pH1-View, SDR_v38	PreSens Precision Sensing GmbH	
nCounter® PanCancer Immune Profiling	NanoString Technologies, Inc.	
PanCancer Pathways	NanoString Technologies, Inc.	
PanCancer Progression Panels	NanoString Technologies, Inc.	
IsoCorrectoR	Bioconductor	https://bioconductor.org/packages/release/bioc/html/IsoCorrectoR.html
Incucyte ZOOM 2018A software	Essen Bioscience	https://www.essenbioscience.com/en/
LabView	National Instruments	https://www.ni.com/de-de/shop/labview/labview-details.html
OriginPro 8.6	OriginLab	https://www.originlab.com
R (3.6.0) survcomp package	Bioconductor	

LEAD CONTACT AND MATERIALS AVAILABILITY

Further information and requests for resources and reagents should be directed to and will be fulfilled by the Lead Contact Dr. Kathrin Renner (Kathrin.Renner-Sattler@ukr.de).

For this study tert-butyl 2-(2-((2,6-dichlorophenyl)amino)phenyl)acetate was synthesized. In the course of collaborations the substance can be provided, however, an MTA is required.

EXPERIMENTAL MODEL AND SUBJECT DETAILS

Mice

Animal experiments on tumors were performed according to the regulations of the local government of Würzburg, Germany and permission was obtained from the Landesuntersuchungsamt Koblenz. C57BL/6J or C57BL/6N mice were purchased from Charles River. For positron emission tomography (PET) and experiments analyzing the impact of drugs on healthy mice or on the growth of B16.SIY wt and B16.SIY LDH$^{-/-}$ tumors, male and female, age-matched (10 – 18 weeks) and sex-matched C57BL/6 mice were used.

To analyze MCT4 deficiency in immune cells *in vitro*, a MCT4$^{-/-}$ mouse model with a C57/BL6J background was used, kindly provided by Prof. Dr. John L. Cleveland (Moffitt Cancer Center and Research Institute, Tampa, FL, USA). Experiments used age-matched and sex-matched littermates.

Experiments analyzing the impact of drugs on tumor growth of 4T1 breast cancer cells were performed with female, 6 - 7 weeks old BALB/c mice (Mark Selby, BMS).

Human Subjects

For analyzing human T cells, the study was approved by the local ethics committee and all human participants gave written informed consent (vote number 13-101-0240; 13-101-0238). Peripheral blood was collected from healthy donors (male and female, 18 to 60 years old) by leukapheresis or directly from leukocyte reduction system cones. For gene expression analysis in human melanoma samples, the study (N03LAM) was approved by the Institutional Ethics Committee (the Netherlands Cancer Institute) and designed and conducted in accordance with the Declaration of Helsinki. All patients gave written informed consent.

Cell Lines and *in Vitro* Cultures

The human cancer cell lines OC316 and IGROV-1 (gifts from Prof. Mueller-Kliesser, Medical University Mainz, Germany), LS174T wt, LS174T MCT knockout clones (Marchiq et al., 2015), and the murine 4T1, B16.SIY wt and LDH$^{-/-}$ cells were cultured in RPMI 1640 (GIBCO, 31870-025), 10% fetal calf serum (Sigma, F7524), 2 mM glutamine (PAN Biotech, P04-80100) in a humidified atmosphere (5% CO_2, 95% air) at 37°C (Heraeus Incubator). The mouse 4T1 tumor cell line was a gift from Prof. F. Balkwill (Barts Cancer Institute, Queen Mary University of London, UK). The B16.SIY LDH$^{-/-}$ was generated as previously described (Ždralević et al., 2018). The PANC-1 cell line was acquired from ATCC. PANC-1-luc cells were generated after transfection with a plasmid encoding for the GFP-luciferase fusion protein (pEGFP-Luc plasmid) and for the G418-resistance gene. The M579-luc melanoma cells were provided by Prof. Michal Lotem (Hadassah Hebrew University Medical Center, Israel) and generated as described (Machlenkin et al., 2008). The PANC-1 and M579-luc cells were cultured in DMEM (high glucose, Sigma-Aldrich, D6429) supplemented with 10% FCS. For experiments, cells were seeded in medium containing 60% DMEM, 30% RPMI 1640, 10% destilled water with 10% FCS. The human melanoma cell line MelIm was a gift from Prof. Dr. Judith Johnson, Institute for Immunology, Munich, Germany in 1993 and was cultured in RPMI.

METHOD DETAILS

Analysis of Gene Expression in Human Melanoma Samples

For this analysis, patients treated with anti-PD-1 as first line checkpoint inhibition and of which pre-treatment tumor material was available were included. All patients gave written informed consent for participation in a biobank study (longitudinal analysis of melanoma-specific immunity in stage III and IV melanoma patients) which was approved by the Institutional Ethics Committee (N03LAM, the Netherlands Cancer Institute) and designed and conducted in accordance with the Declaration of Helsinki. Progression free survival was calculated from date of treatment start to the date of progression or death whichever occurred first. Progression was defined as radiological progression according to immune related response criteria or clinical progression as defined by treating physician when no radiographic imaging was performed before switch off therapy. RNA was isolated from formalin fixed, paraffin embedded pre-treatment tumor samples using the QIAgen AllPrep DNA/RNA kit on the QIAcube according using standard manufacturer's protocol. RNA expression profiling analysis was conducted with the nCounter® PanCancer Immune Profiling, PanCancer Pathways, and PanCancer Progression Panels (Research Use Only. Not for use in Diagnostic Procedures) with custom 30 genes spike-ins for each by NanoString Technologies (Seattle, WA, USA). A glycolytic index was calculated based on co-expression of genes known to be involved in glycolytic metabolism as described in (https://meetinglibrary.asco.org/record/156550/abstract). The numerical index score was calculated from log2 weighted expression of AKT1, HIF1A, SLC2A1, HK1, HK2, TPI1, ENO1, LDHA, PFKFB3, PFKM, GOT1, GOT2, and GLUD1. After calculating the glycolytic/metabolic index, the median expression level was calculated and patients divided into two groups, patients displaying an index below median level and index above median level (n = 23 below; n = 24 above). Kaplan Meier estimation curve was plotted against progression free survival. A multi-variate Cox proportional hazard model was fitted to glycolytic score correcting for sex, age, pre-treatment, stage, and location. All analyses were performed in R (3.6.0) using the survcomp package (Schröder et al., 2011).

Reverse siRNA Transfection of Tumor Cells

Stably luciferase expressing PANC-1-LUC and M579-LUC cells were reverse transfected either with control siRNA (SCR) or siRNAs targeting PD-L1 (siTOOLs Biotech). For siRNA transfection, RNAiMAX (Thermo Fisher Scientific) was used. 10 μL of 50 nM siRNA

solution was added to each well of a 96-well plate. 0.1 μL of RNAiMAX transfection reagent was diluted in 9.9 μL of RPMI (Merck Millipore) and incubated for 10 min at RT. 20 μL of RPMI was added and 30 μL of RNAiMAX mix was given to the wells coated with siRNA and incubated for 30 min at RT. $2x10^3$ PANC-1-LUC cells or 1×10^4 M579-LUC cells were resuspended in 60 μL DMEM medium containing 10% FCS, seeded in the siRNA-RNAiMAX containing wells and incubated for 72 h at 37°C, 5% CO_2. 0.1 mM diclofenac was added to the corresponding wells 4 h after transfection. RNA was isolated using the RNeasy Mini Kit (QIAGEN). Expression of PD-L1 was determined 72 h after transfection by RT-PCR using commercial primers (QIAGEN) and normalized to beta actin (Sigma-Aldrich).

Generation of Flu-Antigen Specific $CD8^+$ T Cells (FluT)

For the generation of influenza (Flu)-specific $CD8^+$ T (FluT) cells, PBMCs from HLA-A*02^+ healthy donors were isolated. Total $CD8^+$ T cells were sorted from PBMCs by magnetic separation and expanded in the presence of A2-matched Flu peptide (GILGFVFTL, ProImmune, Oxford, UK) for 14 d. The autologous $CD8^+$ negative fraction was irradiated and used for 1 week as feeder cells which were then substituted by irradiated T2 cells. On day 1 and day 8, 100 U/mL IL-2 and 5 ng/μL IL-15 (R&D systems) were added. The percentage of Flu-antigen specific T cells were determined by pentamer staining on day 7 and 14. After antigen-specific expansion, FluT cells were sorted by FACS and expanded further for 14 d by using a rapid expansion protocol (https://insights.ovid.com/pubmed?pmid=22421946).

Luciferase-based Cytotoxicity Assay with Influenza-specific $CD8^+$ T cells

After 72 h of transfection with siRNA, PANC-1-LUC and M579-LUC cells were pulsed with 0.01 μg/mL HLA-A*02 matched Flu peptide (GILGFVFTL, ProImmune, Oxford, UK) for 1 h at 37°C, 5% CO_2. After pulsing, peptide-containing media was removed. For cytotoxicity setting transfected cells were cocultured with influenza (Flu)-specific $CD8^+$ T (FluT) cells. For the viability setting T cells or T cell medium alone was added to transfected cells. After 21 h of coculture, supernatant was removed and remaining tumor cells were lysed using 40 μL/well of cell lysis buffer for 15 min. After lysis, 60 μL per well of luciferase assay buffer was added and immediately the luciferase intensity was measured by using a microplate reader (TECAN). Luciferase activity (relative light units = RLUs) was normalized to scramble control. Next, tumor cell viability was calculated as the ratio of luciferase activity of tumor cells only to tumor cells cocultured with FluT cells within one treatment condition.

Real-time Live Cell Imaging

1×10^5 FluT cells were seeded per well in a 96-well flat-bottom plate and kept in 100 μL RPMI medium supplemented with Penicillin/Streptomycin, HEPES, β-mercapthoethanol (all GIBCO) and 10% AB serum (Valley Biomedical) containing the YOYO-1 Iodide dye (491/509, 1:10000, Thermo Fisher Scientific). After seeding, cells were treated either with 0.1 mM diclofenac or with indicated concentrations of lactic acid. Plates were incubated in the Incucyte ZOOM live-cell imager (Essen Bioscience, Welwyn Garden City, UK) at 37°C and 5% CO_2 and images were acquired at the indicated time points. Data were analyzed with the Incucyte ZOOM 2018A software (Essen Bioscience) by generating a top-hat filter-based mask for the calculation the area of YOYO-1 incorporated dead cells.

Determination of MCT Transport Activity

cDNA encoding for rat MCT1 and rat MCT4, respectively, was cloned into the oocyte expression vector pGEM-He-Juel and was transcribed *in vitro* with T7 RNA-Polymerase (Invitrogen Ambion mMessage mMachine, Fisher Scientific, AM1344) as described (Becker et al., 2004, 2014). *Xenopus laevis* females were purchased from *Xenopus* Express (IMP XL FM). Segments of ovarian lobules were surgically removed under sterile conditions from frogs anaesthetized with 1 g/l of 3-amino-benzoic acid ethylester (MS-222, Sigma-Aldrich, E10521), and rendered hypothermic. The procedure was approved by the Landesuntersuchungsamt Rheinland-Pfalz, Koblenz (23 177-07/A07-2-003 §6). As described earlier (Becker et al., 2004, 2014), oocytes were singularized by collagenase (Collagenase A, Roche, 10103586001) treatment in Ca^{2+}-free oocyte saline (pH 7.8) at 28°C for 2 h. The singularized oocytes were left overnight in an incubator at 18°C in Ca^{2+}-containing oocyte saline (pH 7.8) to recover. Oocytes of the stages V and VI were injected with 5 ng of cRNA coding for MCT1 or MCT4. Measurements were carried out 3 to 6 days after injection of cRNA. The oocyte saline had the following composition: 82.5 mM NaCl (Carl Roth, 3957.2), 2.5 mM KCl (Sigma Aldrich, 60130), 1 mM $CaCl_2$ (Merck, A935182), 1 mM $MgCl_2$ (Merck, A748033), 1 mM Na_2HPO_4 (Sigma Aldrich, 30427), 5 mM HEPES (Carl Roth, 9105.3); titrated with NaOH (Carl Roth, 9356.1) to pH 7.0. In lactate-containing saline, NaCl was substituted by Na-L-lactate (Sigma Aldrich, 71718) in equimolar amounts. NSAIDs were dissolved in ddH_2O and added to the saline shortly before the experiment. MCT transport activity in oocytes was determined by measuring changes in intracellular H^+ concentration with ion-sensitive microelectrodes under voltage-clamp conditions, using single-barreled microelectrodes (Becker et al., 2004, 2014; Bröer et al., 1999; Deitmer, 1991; Dimmer et al., 2000). The manufacture and application have been described in detail previously (Becker, 2014; Deitmer, 1991). As described (Bröer et al., 1999), optimal pH changes were detected when the electrode was located near the inner surface of the plasma membrane. During all measurements, oocytes were clamped to a holding potential of −40 mV using an additional microelectrode, filled with 3 M KCl and connected to an Axoclamp 2B amplifier (Axon Instruments). All experiments were carried out at room temperature. The measurements were stored digitally using custom-made PC software based on the program LabView (National Instruments). The rate of change of the measured $[H^+]_i$ ($\Delta[H^+]/\Delta t$) was analyzed by determining the slope of a linear regression fit using

OriginPro 8.6 (OriginLab). Conversion and analysis of the data have been described in detail previously (Becker, 2014). For determination of IC_{50} values transport activity of MCT1 and MCT4 was first determined by measuring $\Delta[H^+]/\Delta t$ during application of 3 and 10 mM lactate, respectively. The two concentrations were chosen according to the transporters K_m values (Dimmer et al., 2000). After washout of lactate the NSAID was applied for 10 min before application of lactate in the presence of NSAID. To determine the effect of a given NSAID concertation on MCT activity, $\Delta[H^+]/\Delta t$, induced by the lactate pulse in the presence of NSAID was calculated as % of the $\Delta[H^+]/\Delta t$ induced by the lactate pulse in the absence of NSAID in the same cell. This procedure was carried out five times for every NSAID concentration. The resulting data points were fitted with a Hill equation using OriginPro 8.6.

T Cell Isolation, Stimulation and Culture

Human T cells: Peripheral blood mononuclear cells were isolated by density gradient centrifugation over Ficoll/Hypaque as described (Andreesen et al., 1990) and T cells were isolated by magnetic bead separation. T cell purity was >98% determined by CD4 (BD Bioscience) and CD8 (BioLegend) expression by flow cytometry. T cells were cultured in RPMI 1640 (GIBCO, 31870-025) or RPMI 1640 without glucose (Sigma-Aldrich, R1383-1L) supplemented with 10% human AB serum (BRK, Bavarian Red Cross), 2 mM L-glutamine (PAN-Biotech, P04-80100), essential vitamins (GIBCO, 1112037) and non-essential amino acids (GIBCO, 11140035), 1 mM pyruvate (GIBCO, 11360039), β-mercapthoethanol (GIBCO, 31350010), penicillin and streptomycin (both GIBCO, 15140122) and 25 IU/mL rhIL-2 (PeproTech, 200-02) in a humidified atmosphere (5% CO_2, 95% air) at 37°C in a Heraeus incubator. 0.1×10^6 cells T cells were seeded in 96-well U-bottom plates and either stimulated with anti-CD3/CD28 dynabeads (Thermo Fisher Scientific) at a cell to bead ratio of 1:1 or in a mixed lymphocyte reaction (MLR) with 0.01×10^6 allogeneic mature dendritic cells (DCs). Bead stimulated T cells were fed at day 3. For re-stimulation T cell population beads were removed after 6 d of stimulation, T cells were washed and re-stimulated following the same protocol as during stimulation. Immature DCs were differentiated from monocytes, isolated from PBMCs of healthy donors after leukapheresis followed by density gradient centrifugation over Ficoll/Hypaque. Monocyte purity was >85% determined by CD14 expression. 0.7×10^6/mL monocytes were cultured in RPMI 1640 supplemented with 50 U/mL penicillin, 50 mg/mL streptomycin, 2 mM L-glutamine, 10% FCS (Sigma, F7524), 144 U/mL IL-4 (Peprotech, 200-04,) and 225 U/mL GM-CSF (Peprotech, 300-03). On day 5, 100 ng/mL LPS (Enzo, ALX-581-009-L002) were added to induce maturation of DCs. NSAIDs and MCT inhibitors were added to T cell cultures simultaneously with stimulus, and the drug concentrations were kept constant when fresh medium was added.

Murine T cells: Spleens of WT and $MCT4^{-/-}$ mice were scratched out to gain splenocytes in a single-cell suspension and erythrocytes were removed with ACK lysis buffer (0.155 M NH_4Cl, 0.1 M $KHCO_3$ and 0.1 mM EDTA, diluted 1:6 with H_2O). Splenocytes were stored for at least 2 h in a humidified atmosphere (5% CO_2 at 37°C). Murine T cell populations were isolated by magnetic bead separation (Miltenyi Biotec) and cultured in RPMI composed similar to the RPMI for human T cells (with the exception that 10% FCS were used instead of AB serum).

0.2×10^6 T cells were stimulated with anti-CD3e (coated, 5 μg/mL, BD Biosciences) in combination with anti-CD28 antibody (soluble, 1 μg/mL, BD Biosciences). T cells were cultured with rhIL-2 (end concentration of 10 U/mL, PeproTech) in 200 μL medium in a 96-well flat bottom plate resulting in a cell concentration of 1.0×10^6 cells per mL and incubated in a humidified atmosphere (5% CO_2) at 37°C. Diclofenac and SR13800 were added to T cell cultures simultaneously with stimulus.

In Vitro Analysis of $CD8^+$ T Cells Cocultured with B16.SIY Tumor Cells

The effect of diclofenac on checkpoint inhibition *in vitro* was analyzed using 2C TCR transgenic $CD8^+$ T cells recognizing the SIY peptide in association with H2Kb. For coculture experiments, $CD8^+$ T cells were isolated from spleens of 2C/Rag2−/− mice by magnetic bead separation (Miltenyi Biotec). Purified 2C $CD8^+$ T cells (1×10^5) were stimulated twice with irradiated (20 Gy) P815.B7-1 mastocytoma cells (5×10^5) in RPMI with IL-2 (10 U/mL). After 11 d stimulated $CD8^+$ T cells were collected and purified by density gradient centrifugation.

0.25×10^5 B16.SIY cells were cultured with or without 20 ng/mL murine IFNγ (Pepro Tech) in 96-well plates for 24 h to induce an upregulation of SIY/H2Kb with and without 0.1 mM diclofenac. After washing the wells with medium (3x), supernatants from cells cultured without IFNγ in the presence of diclofenac were transferred to the IFNγ treated B16.SIY cells together with 0.5×10^5 stimulated 2C $CD8^+$ T cells in the presence of anti-PD-1 (10 μg/mL, BioLegend) or isotype control (10 μg/mL, BioLegend). Supernatants were harvested to analyze IFNγ levels after 24 h.

Determination of Cell Size and Cell Number

Cell number and size were determined using the CASY system (Omni Life Science).

Determination of Cytokines

Cytokine secretion was determined in 48 h culture supernatants by commercially available enzyme-linked immunosorbent assays (R&D Systems) according to the manufacturer's protocol.

Determination of Glucose Metabolism

For determining glucose uptake and lactate secretion of tumor cell lines, 0.025×10^6 cells were seeded in 200 μL medium in 96-well plates in the presence or absence of NSAIDs and MCT inhibitors and supernatants were taken after overnight cultures. Glucose

metabolism of human and murine T cells was analyzed in culture supernatants after 48 h of activation, as after 24 h lactate secretion is not detectable. Medium glucose and lactate levels were measured enzymatically and concentration calculated by standard curves. Glucose concentration was measured by a commercially available kit (Sigma-Aldrich), lactate concentration was determined using a Dimension Vista (Siemens,) and specific reagents (Roche Innovatis) at the Department of Clinical Chemistry, University Clinic, Regensburg, Germany. All values were corrected for lactate concentration of the culture medium.

$^{13}C_6$-Glucose Tracer Analysis

To perform $^{13}C_6$-Glucose tracing in T cell activation, human $CD4^+$ and $CD8^+$ T cells were stimulated with anti-CD3/CD28 dynabeads for 6 d. At day 6, T cells were pooled, washed with glucose-free medium and re-stimulated with anti-CD3/CD28 dynabeads in the presence of 0.1 and 0.2 mM diclofenac or 0.2 mM ketoprofen and 10 mM $^{13}C_6$ glucose (Cambridge Isotope Labs). Cells were cultured for 48 h in the presence of the indicated compounds, washed 2x in PBS, and immediately frozen. Cell pellets were kept at −80°C until further analysis. Experiments were performed with cells from 3 different donors. Metabolite extraction was performed with 80% methanol. Amino acids isotopologues were analyzed by high performance liquid chromatography (HPLC)–electrospray ionization (ESI)–tandem MS (MS/MS) after propyl chloroformate derivatization and intermediates of glycolysis and TCA cycle by GC-MS after derivatization using methoximation and silylation (Feist et al., 2018; Loftus et al., 2018). All raw data were corrected for natural stable isotope abundance and tracer impurity using IsoCorrectoR (Heinrich et al., 2018). Data are presented as mean isotopic enrichment.

Western Blot Analysis

Cell samples were lysed in RIPA-buffer (Sigma-Aldrich), separated by 12% SDS-PAGE and transferred to PVDF membranes, blocked with 5% milk (Sucofin) in TBS buffer with 0.1% Tween for 1 h, and incubated with primary antibodies overnight. Primary antibodies: MCT1 (Thermo Fisher Scientific, Santa Cruz Biotechnologies), MCT4 (Santa Cruz Biotechnologies), GLUT1 (Abcam), LDHA (Cell Signaling), LDHB (Santa Cruz Biotechnologies), β-Actin (Sigma-Aldrich). Membranes were incubated with the following secondary antibodies for 1 h at RT: Goat anti-rabbit HRP (Agilent), Goat anti-mouse HRP (Agilent). Detection was performed by chemiluminescence (ECL, Amersham Bioscience, RPN2232) and analyzed using the chemiluminescence system Fusion Pulse 6 (Vilber Lourmat). For detection of multiple antigens, antibodies were removed from the membrane by incubation with ReBlot Plus Strong Stripping Solution (Merck, 2504) for 15 min.

Monitoring of Oxygen Consumption and pH Development *in Vitro*

Cellular oxygen consumption and pH changes in culture medium were determined non-invasively by the PreSens technology (PreSens Precision Sensing GmbH). 0.2×10^6 tumor cells or 0.8×10^6 T cells with anti-CD3/CD28 dynabeads (with a cell to bead ratio of 1:1, Thermo Fisher Scientific) were seeded in 24-well Oxodish® OD24 or Hydrodish® HD24 plates without fixation in 1 mL medium under cell culture conditions for the indicated period of time.

Determining Tumor pH

Tumor pH was determined in size matched tumors by a micro fiber optic pH meter with needle-type housed pH microsensors (20/0.4) using a manual micromanipulator (PreSens Precision Sensing GmbH). Vehicle, diclofenac or lumiracoxib were administered 2 h prior to pH measurement. Microsensors were calibrated for at least 30 min, tumors were dissected and pH microsensor was inserted 1 or 2 mm into the tumor and pH was reported in between one to three min with the software pH1-View.

^{18}F-FDG micro-PET/magnetic Resonance Imaging

PET imaging was performed according to Bohn et al. (2018). All mice used for this study were bred and housed at the animal facility of Johannes Gutenberg University using institutionally approved protocols (permission was obtained from the Landesuntersuchungsamt Koblenz). In short, tumor-bearing mice were injected intravenously with 6.3 ± 0.5 MBq ^{18}F-FDG followed by a 60 min uptake period. Mice were anesthetized with isoflurane and measurements were performed followed by a 15 min static PET scan.

Preparation of Mouse Tissue for Flow Cytometry

Spleen was minced in RPMI 1640 supplemented with 10% FCS and 2 mM glutamine and was centrifuged after filtration through a 100 μm cell strainer. Tumors were minced and incubated with Deoxyribonuclease I and Collagenase IA (Sigma-Aldrich) in RPMI 1640 supplemented with 10% FCS for 1 h at 37°C, passed through a 70 μm cell strainer and centrifuged. Erythrocytes in single cell suspensions of tumors and spleens were lysed with ACK lysis buffer 1X (6X: 0.155 M NH_4Cl, 0.01 M $KHCO_3$ and 0.1 mM EDTA) for 3 min at RT. For blood samples lysis with ACK lysis buffer was performed for 5 min at RT after a washing step with flow cytometry buffer (PBS containing 2% FCS). All samples were then washed with flow cytometry buffer and cells were further passed through a 100 μm cell strainer. $1 - 3 \times 10^6$ cells were used for flow cytometry staining.

Flow Cytometry

Human T cell populations were stained with anti-CD4 (BD Biosciences), anti-CD8 (BioLegend), anti-CD25 (BD Biosciences), anti-CD137 (Thermo Fisher Scientific) and anti-PD-1 (BioLegend). Quiescent T cells or isotype control were used as negative controls.

For analyzing surface markers on tumor cells, human and murine tumor cells were seeded into 6-well plates (0.15×10^6 cells per well in 5 mL) for 72 h. Murine tumor cells were stimulated with 20 ng/mL IFNγ (PeproTech) and cells were stained with anti-I-Ab (for B16.SIY, BioLegend), anti-I-A/E (for 4T1, BioLegend), anti-H-2Kb (for B16.SIY, BD Biosciences), anti-H-2Dd (4T1, BioLegend) and anti-PD-L1 (BioLegend). Human tumor cells were stained using anti-HLA-ABC (MHC I, BD Biosciences) and anti-PD-L1 (BioLegend). Apoptosis was determined by Annexin-V/ 7-AAD staining (BD Biosciences).

Single cell suspension was generated from tumor, blood, spleen, and lymph nodes of C57/BL6 and BALB/c mice. After manufacturing single cell suspensions, cells were treated with FcR-blocking reagent (Miltenyi Biotec) for 10 min at 4°C after washing with flow cytometry buffer. To exclude dead cells, samples were washed twice with PBS and incubated with 70 μL Zombie NIR dye (solved in 100 μL DMSO and diluted 1:650 with PBS, BioLegend) for 10 min at RT in the dark. Next, cells were stained with anti-CD3e (Thermo Fisher Scientific or BD Biosciences), anti-CD4 (Thermo Fisher Scientific or BioLegend), anti-CD8a (BD Biosciences or Miltenyi Biotec), anti-CD45 (BD PharMingen or Miltenyi Biotec), anti-NK1.1 (Biolegend or Thermo Fisher Scientific), and anti-IFNγ (BioLegend). Intracellular staining of IFNγ was performed after incubation of single cell suspensions with BD GolgiStop (BD Biosciences) in medium for 2 h at 37°C using the Intracellular Fixation and Permeabilization Buffer Set (Thermo Fisher Scientific) according to the manufacturer's protocol. Flow cytometry was performed using a BD FACS Calibur, LSR Fortessa or LSR II instrument (BD Biosciences). Data were analyzed with the FlowJo software (Tree Star Inc, version 9.9.6 or 10.4.1).

Syngeneic Tumor Models

To generate B16 tumors in mice, B16.SIY wt or B16.SIY LDH$^{-/-}$ cells were harvested, washed and 1.0 or 0.3×10^5 tumor cells were injected in 50 μL RPMI medium or in RPMI with ECM (1:2) subcutaneously in the dorsal region of mice. Diclofenac was solved in 0.9% NaCl, lumiracoxib in DMSO and diluted with medium (1:20). NSAIDs were administered intraperitoneally (i. p.) every day, anti-PD1 (Leinco or Bio X Cell) and anti-CTLA-4 (Bio X Cell) antibodies were administered at a concentration of 10 mg/kg every 3rd day beginning at day 4 to 6.

For PET analysis 2.0×10^5 B16.SIY wt or B16.SIY LDH$^{-/-}$ cells (in 100 μL PBS) were injected subcuteanously into the right (wt) or left (LDH$^{-/-}$) flank of C57BL/6J mice. 16 d after tumor cell inoculation glucose uptake of B16.SIY wt and B16.SIY LDH$^{-/-}$ tumors was measured by PET.

4T1 breast tumor cells were harvested from subconfluent monolayers, washed and 1×10^6 cells were injected in 100 μL of PBS or 50 μL RPMI medium with ECM subcutaneously into syngeneic BALB/c mice. Diclofenac was injected i. p. twice daily at 7.5 mg/kg for 14 d and started on day 6. Aspirin dosing was performed by addition to the drinking water at 600 μg/mL, beginning on day 6 and was replenished every 3 d. Anti-PD1 (clone 4H2) and anti-CTLA-4 (clone 9D9) antibodies were administered at a concentration of 10 mg/kg every 3-4 day for one week started on day 6.

Tumor volumes were estimated by measurements of the short (a) and long (b) axis of the mass and the following formula: $V = \pi/6 \times 0.5 \times a \times b$. Animals were monitored daily for tumor size and their general condition. At indicated time points mice were killed and blood, spleens, and tumors of mice bearing tumors with a max. size of 1000 mm^3 were prepared for analysis.

Histology

General histological analyses were performed of different treated mice (n = 29, B16.SIY wt: control n = 6, checkpoint n = 6, diclofenac n = 3, diclofenac + checkpoint n = 7, lumiracoxib n = 2, lumiracoxib + checkpoint n = 5; n = 13 B16.SIY LDH$^{-/-}$: control n = 5, checkpoint n = 8). Stomach, liver, kidneys, lung, ovaries, heart, pancreas, small and large bowel, bone marrowand lymph nodes (lymph nodes only if macroscopical suspicious) were analyzed histologically. After fixation in buffered formalin the samples were dehydrated by standard techniques and embedded in paraffin. Slides of 3 - 5 μm were cut with a microtome and hematoxylin and eosin (HE) staining was performed following general protocols.

Synthesis of tert-butyl 2-(2-((2,6-dichlorophenyl)amino)phenyl)acetate (Diclofenac tert-butyl ester, DtBE)

The synthesis was done by an esterification method using sulfuric acid/$MgSO_4$ (Qin and Davies, 2013). Anhydrous $MgSO_4$ (289 mg, 2.40 mmol, 4.0 eq, VWR, 33337.A3) and dry CH_2Cl_2 (MERCK, 1060502500) were placed in a 100 mL round-bottom flask. Sulfuric acid (31.9 μL, 58.8 mg, 0.600 mmol, 1.0 eq, MERCK,1007312500) was added, and the mixture stirred for 30 min at room temperature. Subsequently, diclofenac sodium salt (191.0 mg, 0.600 mmol, 1.0 eq) and *t*BuOH (281 μL, 222 mg, 3.00 mmol, 5.0 eq, CARL ROTH, AE16.2) were added. The reaction mixture was refluxed (45°C) overnight, before after 20 h another 289 mg (2.40 mmol, 4.0 eq) of $MgSO_4$ and *t*BuOH (281 μL, 222 mg, 3.00 mmol, 5.0 eq) were added and the mixture refluxed for further 7 h. The resulting mixture was cooled, then filtered and neutralized with saturated aqueous $NaCO_3$ (MERCK, 1063920500) solution. After separation of the layers, the organic layer was washed with brine (3 × 30 mL) and dried over $MgSO_4$. Finally, the solvent was removed under reduced pressure, the residue taken up in MeOH (MERCK, 1060092511) and purified by preparative TLC (SiO_2, PE/EA 9:1 (v/v)) to yield Diclofenac *tert*-butyl ester (DtBE) (21.1 mg, 0.0600 mmol, 10%) as colorless oil. R_f = 0.89 (SiO_2, PE/EA 3:2 (v/v)); ^{1}H-NMR (400 MHz, Methanol-d_4): δ = 7.40 (d, *J* = 8.1 Hz, 2H, C*H*$_{arom}$), 7.19 (d, *J* = 7.4 Hz, 1H, C*H*$_{arom}$), 7.07 (t, *J* = 8.1 Hz, 2H, C*H*$_{arom}$), 6,91 (t, *J* = 7.5, 1H, C*H*$_{arom}$), 6.42 (d, *J* = 8.0 Hz, 1H, C*H*$_{arom}$), 3.70 (s, 2H, C*H*$_2$), 1.47 (s, 9H, CH(C*H*$_3$)$_3$); ^{13}C-NMR (101 MHz, Methanol-d_4, DEUTERO GMBH, 01105): δ = 173.5, 144.2, 144.1, 139.3, 131.9, 131.1, 130.1, 128.8, 126.3, 125.7, 122.9, 118.8, 82.6, 40.5, 28.3; LR-MS (APCI-MS) m/z (%): 352.1 [MH$^+$]; HR-MS (ESI-MS): calcd for $C_{18}H_{20}Cl_2NO_2$ [MH$^+$] 352.0866, found 352.0875. ^{1}H NMR spectra were recorded on a Bruker (Billerica, Massachusetts, USA) spectrometer Avance 400 (400 MHz). Chemical shifts

δ are referenced to methanol-d_4 (3.31 ppm, DEUTERO GMBH, 01105-10ml) and reported in ppm, coupling constants in Hz. Multiplets are abbreviated as: s = singlet, d = doublet, t = triplet. ^{13}C NMR spectra were recorded on Avance 400 (101 MHz) spectrometer with chemical shifts δ in ppm that are referenced to methanol-d_4 (49.0 ppm). Mass data were obtained on Agilent Technologies 6540 UHD (Santa Clara, USA), Finnigan MAT 95 or Thermo Quest Finnigan TSQ 7000 instruments (Bremen, Germany). All reagents were purchased from commercial sources and were used without further purification. Solvents were distilled before use. Reactions were carried out under nitrogen gas and the glassware was heated at 110°C before use when dry conditions were necessary. The reactions were monitored by TLC on silica gel plates 60 F254 by MERCK (Darmstadt, Germany). Spots were detected under UV light (λ = 254 and 366 nm). Preparative TLC plates were set up using silica gel 60 GF254 by MERCK (Darmstadt, Germany).

Chemicals

Unless noted otherwise all chemicals were dissolved in water. Diclofenac was dissolved in RPMI 1640 (Sigma-Aldrich, D6899, stock concentration 8 mM, final concentration 0.1 or 0.2 mM), ketoprofen in ethanol (Sigma-Aldrich, 471909, stock concentration 10 mM, final concentration 0.1 or 0.2 mM), the MCT1/2 inhibitors AZD3965 in DMSO (Tocris, 4960, stock concentration 10 mM, final concentration 0.1 μM) and SR13800 (stock concentration 10 mM, final concentration 0.1 μM, gift from Prof. Cleveland) in DMSO (Honeywell Research Chemicals, 34869), acetyl salicylic acid in RPMI 1640 (Fagron, 701627-0003, stock concentration 20 mM, final concentration 1 mM). DMSO was applied as carrier control when appropriate.

QUANTIFICATION AND STATISTICAL ANALYSIS

Statistical parameters including the exact value of n, the definition of the center, dispersion, and precision and statistical significance are reported in the figures and the figure legends. Statistical analysis was performed with the GraphPad Prism software (version 7 or 8). Data are judged to be statistically significant when $p < 0.05$ by one-way ANOVA and Tukey's or Dunnett's multiple comparisons test for comparison of more than two groups as well as paired or unpaired/two-tailed Mann-Whitney U test for comparison of two groups. Significance between the melanoma patient groups with a low or high glycolytic index was calculated applying the Log-rank (Mantel-Cox) test. In figures asterisks denote statistical significance (* $p < 0.05$, ** $p < 0.01$, *** $p < 0.001$). Multifactorial analyses of patient data including sex, age, location, and stage were performed with the software package R (3.6.0) survcomp package

DATA AND CODE AVAILABILITY

There are restrictions to the availability of the human dataset on the correlation of anti-PD-1 treatment response and glycolytic index as these are patient data and thus are subject to data protection.